

**STUDY ON THE PHOTOINDUCED MORPHOLOGICAL
CHANGES IN AZOBENZENE-CONTAINING LIQUID
CRYSTALLINE THIN FILMS**

LI Wenhan

**STUDY ON THE PHOTOINDUCED MORPHOLOGICAL
CHANGES IN AZOBENZENE-CONTAINING LIQUID
CRYSTALLINE THIN FILMS**

LI Wenhan

李文瀚

Molecular Design and Engineering
Nagoya University

2012

Contents

Chapter 1	4
General Introduction	4
1.1 Azobenzene	4
1.1.1 Historical background	4
1.1.2 Chemical structure and behavior	5
1.1.3 Trans-cis isomerization	5
1.1.4 Spectroscopic classification	6
1.1.5 Photo physics of isomerization	6
1.2 Photoinduced motions of azobenzene	8
1.2.1 Historical background of azo motions	8
1.2.2 SRG on an amorphous azo polymer	9
1.2.3 SRG of liquid crystalline Azo polymer	12
1.2.4 Limitation of current SRGs	17
1.2.5 Application of SRG	19
1.3 Purpose of this research	19
References	21
Chapter 2	24
Photo-crosslinkable Liquid-crystalline azo-polymer for Surface Relief Gratings and Persistent Fixation	24
2.1 Introduction	24
2.1.1 Chemical crosslinking	25
2.1.2 Photo-initiated crosslinking	25
2.2 Experimental	28
2.2.1 Synthesis of 4-[(4'-pentyl)azo]phenol (5Az-OH)	28
2.2.2 Synthesis of 4-(10-hydroxydecyl)-4'-pentylazobenzene (5Az10-OH)	30
2.2.3 Synthesis of 4-(10-methacryloyloxydecyloxy)-4'-pentylazobenzene (5Az10Me)	30
2.2.4 Polymerization of p5Az10Me-PE4.5	33
2.2.5 Synthesis of p5Az10Me-PE4.5-Ci	33
2.2.6 Gel permeation chromatography (GPC) measurements	35
2.2.7 DSC measurements	35
2.2.8 Polarized optical microscopic (POM) measurements	37
2.2.9 UV-vis absorption spectra measurements	37
2.2.10 Film fabrication	37
2.2.11 SRG formation	39
2.2.12 AFM observation	41

4.2.2 Methods	75
4.3 Results and discussion	77
4.3.1 Thickness dependent hierarchical SRG	77
4.3.2 Thickness dependent dewetting of D6	80
4.3.3 Mechanism assumption	83
4.4 Conclusions	86
References	87
Chapter 5	88
Summary	88
Publication List	90
Acknowledgments	91

Chapter 1

General Introduction

1.1 Azobenzene

1.1.1 Historical background

Azobenzene derivatives have been studied extensively for a long time. The earliest and widest applications are in the use for dye-stuffs because a variety of colors could be obtained depending on their chemical structure. Also, the photo-isomerization of azobenzene has long been the subject of great interest. Nevertheless, in the last 20 years, azobenzene chemistry has been expanding with an amazing output of novel phenomena. The main reason for this can be the invention of laser light, which allows focused addressing of variable intensities. When an azobenzene group is incorporated into various matrixes, its photo-isomerization can cause a wide range of unexpected consequences. For instance, Todorov *et al.*^[3] have mentioned and explained the orientation of azobenzene groups dissolved in a polymer film perpendicular to the laser beam polarization direction. A polarized light can induce significant orientation of these molecules, which lead to dichroism and birefringence.

The following sections will give a general overview of the researches of photo-induced motions in azobenzene containing polymer films triggered by photoisomerization of azobenzene. Finally, our recent studies on photo-induced surface relief gratings are reviewed to give the motivation of this thesis.

1.1.2 Chemical structure and behavior

Azobenzene is a chemical compound composed of two phenyl rings linked by a N=N double bond. The term 'azobenzene' or simply 'azo' is often used to refer to a wide class of molecules that share the core azobenzene structure, with different chemical functional groups extending from the phenyl rings. These compounds should be formally referred to as 'diazenes'. The diazenes strongly absorb light and were historically used as dyes in a variety of industries.

Azobenzene was first described in 1856 as "gelblich-rothe krystallinische Blättchen".^[1] Its original preparation is similar to the modern one. According to the 1858 method, nitrobenzene is reduced by iron filings in the presence of acetic acid. In the modern synthesis, zinc is the reactant in the presence of base.^[2]

1.1.3 Trans-cis isomerization

One of the most intriguing properties of azobenzene (and derivatives) is the photoisomerization of trans and cis isomers. The two isomers can be switched with particular wavelengths of light: ultraviolet light, which corresponds to the energy gap of the π - π^* (S2 state) transition, for trans-to-cis conversion, and blue light, which is equivalent to that of the π - π^* (S1 state) transition, for cis-to-trans isomerization. For a variety of reasons, the cis isomer is less stable than the trans (for instance, it has a distorted configuration and is less delocalized than the trans configuration). Thus, cis-azobenzene will thermally relax back to the trans via cis-to-trans isomerization. The trans isomer is more stable by approximately 50 kJ/mol, and the barrier to photo-isomerization is approximately 200 kJ/mol.

1.1.4 Spectroscopic classification

The wavelength at which azobenzene isomerization occurs depends on the particular structure of each azo molecule, but they are typically grouped into three classes: the azobenzene-type molecules, the amino azobenzenes, and the pseudo-stilbenes. These azos are yellow, orange, and red, respectively, owing to the subtle differences in their electronic absorption spectra. The compounds similar to the unsubstituted azobenzene exhibit a low-intensity $n-\pi^*$ absorption in the visible region, and a much higher intensity $\pi-\pi^*$ absorption in the ultraviolet. Azobenzene that are ortho- or para-substituted with electron-donating groups (such as aminos), are classified as aminoazobenzenes, and tend to closely spaced $n-\pi^*$ and $\pi-\pi^*$ bands in the visible. The pseudo-stilbene class is characterized by substituting the 4 and 4' positions of the two azo rings with electron-donating and electron-withdrawing groups (that is, the two opposite ends of the aromatic system are functionalized). The addition of this push-pull configuration results in a strongly asymmetric electron distribution, which modifies a host of optical properties. In particular, it shifts the absorption spectra of the *trans* and the *cis* isomers, so that they effectively overlap. Thus, for these compounds a single wavelength of light in the visible region will induce both the forward and reverse isomerization. Under illumination, these molecules cycle between the two isomeric states.

1.1.5 Photo physics of isomerization

The photo-isomerization of azobenzene is extremely rapid, occurring on picosecond timescales. The rate of the thermal back-relaxation varies greatly depending on the compound: usually hours for azobenzene-type molecules, minutes for aminoazobenzenes, and seconds for the pseudo-stilbenes.

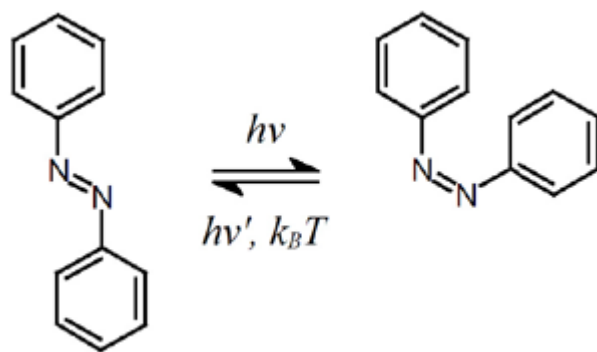


Figure 1-1. Azobenzene photoisomerization.

The mechanism of isomerization has been the subject of some debate, with two pathways identified as viable: a rotation about the N-N bond, with disruption of the double bond, or via an inversion, with a semi-linear and hybridized transition state. It has been suggested that the trans-to-cis conversion occurs via rotation into the S₂ state, whereas inversion gives rise to the cis-to-trans conversion. It is still under discussion which excited state plays a direct role in the series of the photoisomerization behavior. However, One research on femtosecond transition spectroscopy has suggested that the S₂ state undergoes internal conversion to the S₁ state, and then the trans-to-cis isomerization proceeds. In year 2004, another isomerization pathway has been proposed by Diau, the "concerted inversion" pathway in which both CNN bond angles bend at the same time.

1.2 Photoinduced motions of azobenzene

1.2.1 Historical background of azo motions

The photo-isomerization of azobenzene is a form of light-induced molecular motion. This isomerization can also lead to motion on larger length scales. For instance, polarized light will cause the molecules to isomerize and relax in random positions. However, those relaxed (trans) molecules that fall perpendicular to the incoming light polarization will no longer be able to absorb, and will remain fixed. Thus, there is a statistical enrichment of chromophores perpendicular to polarized light (orientational hole burning). Polarized irradiation will make an azo-material anisotropic and therefore optically birefringent and dichroic. This photo-orientation can also be used to orient other materials (especially in liquid crystal systems)^{[4][10]}. For instance, it has been used to selectively orient liquid crystal domains, and used to create nonlinear optical (NLO) materials. Azo isomerization can also be used to

photo-switch the liquid crystal phase of a material from cholesteric to nematic^{[5][6]} or to change the pitch of a cholesterol phase.^[7]

In 1995, it was reported that exposing a thin film of azo-polymer to a light intensity (or polarization) gradient leads to spontaneous surface patterns.^{[8][9]} In essence, the polymer material will reversibly deform so as to minimize the amount of material exposed to the light. This phenomenon is not laser ablation, since it readily occurs at low power and the transformation is reversible. This detailed mechanism of this surface holography is still unresolved, although it is clearly related to the azobenzene isomerization.

Bulk expansion and contraction of azobenzene materials have also been observed. In one report, a thin film was made to bend and unbend by exposing it to polarized light. The direction of the macroscopic motion could be controlled by the polarization direction. The bending occurred because the free surface of the material contracted more than the inside of the thin film (due to absorption of laser light as it passes through the film).

1.2.2 SRG on an amorphous azo polymer

Since the work of Todorov in year 1984,^[3] birefringence gratings on azobenzene-based polymers have been studied. This type of grating formation originates in general from a spatially periodic change in photo-induced orientation state. Aside from this, irradiation of the azobenzene containing amorphous polymer films for a period of time longer than that required for photo-induced orientation was found to produce an unexpected modification of the film surface (**Figure 1-2**). Such large surface relief modulation is attributed to mass transport over micrometer distances. The mass transport process has been accomplished with irradiation at a

modest light intensity and at ambient temperature, significantly below the glass transition temperature. The formation of such surface relief grating (SRG) on the films was firstly published independently in 1995 by Kim^[9] and Rochon^[8]. Since the discovery, studies on SRG have formed a fascinating research area of azobenzene polymer chemistry due to the basic phenomenological interests and attractive technological possibility. A periodicity and height of the inscriptions can be actually controlled on-demand by irradiating conditions regarding an interference angle, exposure energy and polarization combinations of writing beams.

There are some papers reviewing surface relief gratings research describing both the mechanism and their possible photonic applications. Various theoretical models have been proposed to account for the mechanism of light-driven mass transport. For *amorphous* azobenzene-containing polymer films, the model proposed by Tripathy's group (*field gradient force model*) seems the most plausible and can explain the polarization dependence observed for photoinduced mass transfer.^[12] The force comes from a combination of the change in the electric susceptibility and the field gradient. Optically induced changes in electric susceptibility depend on the direction of the total electric field. In addition, the dipole interaction between the optical field and an azobenzene chromophore induces a change in the electric susceptibility, which is due to photo-induced dichroism and birefringence. A clear feature of the photo-induced mass transfer in amorphous azobenzene polymers is that the force only works in the direction of the field gradient. However, there are still many issues to be solved with regard to the mechanism, which also seems to be material dependent. For instance, Ramanujam *et al.* reported a unique phenomenon. Most of the literature reports seem to agree that the material is displaced from the area of most intense illumination. However, this appears to

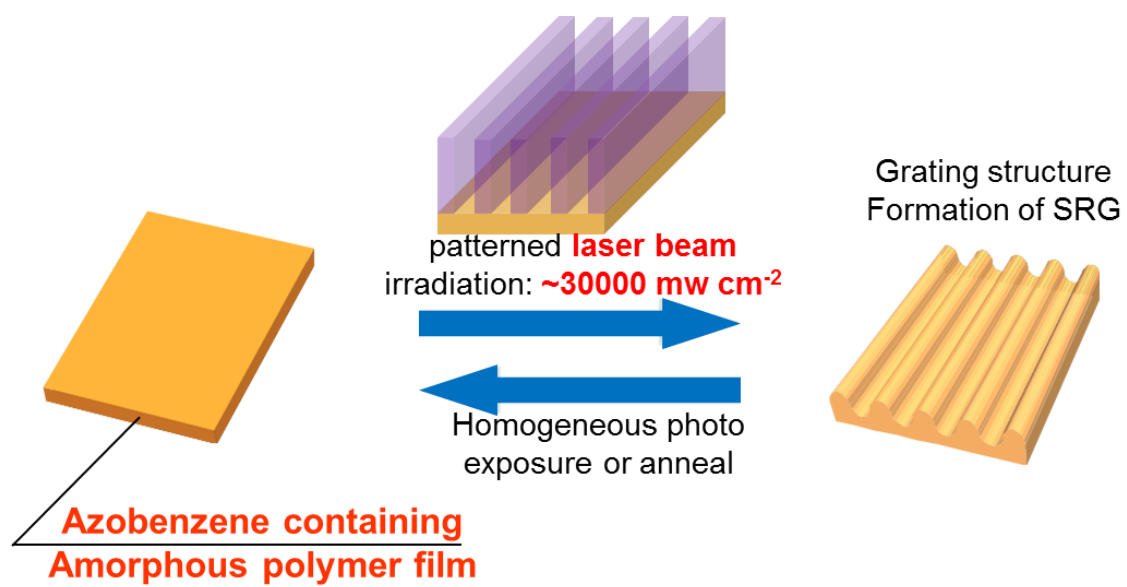


Figure 1-2 Photo induced surface relief gratings

depend on the polymer structure because there is one example that peaks instead of trenches, are obtained for a particular liquid crystalline polymer. In an attempt to explain this behavior, the authors have conducted an experiment in which they illuminated linearly polarized light onto a film floating on water.^[12] They show that liquid crystalline polymer films behave differently from an amorphous film.

1.2.3 SRG of liquid crystalline Azo polymer

When a substrate surface is chemically modified with photochromic residues of azobenzene, macroscopic alignment of low-molecular-weight nematic liquid crystal (NLC) molecules can be manipulated by alternate irradiation with UV and visible light which induce alternate isomerization between rod-like trans and bended cis forms. The first observation and the extensions of research in this area were mostly performed at Ichimura's group.^{[4][13]} They coined the 'command surface' concept. The most interesting aspect of this process is one can calculate that ca. $10^4 \sim 10^5$ NLC molecules are driven by only two azobenzene groups.^[13]

There are four modes of the NLC alignment controls by command surface effects; (i) out-of-plane alignment between homeotropic and planer mode,^[13] (ii) out-of plane alignment between homeotropic and homogeneous mode,^[14] (iii) in-plane alignment by irradiation with linearly polarized light,^{[15][16]} (iv) three-dimensional alignment by slantwise irradiation with non-polarized light.^[17] Systematic studies on the command surface allowed the potential application to other types of liquid crystalline materials involving smectic,^[18] cholesteric,^[19] discotic,^[20] lyotropic,^[21, 22] and polymer liquid crystallines.^[18] An excellent review covering the photo-alignment in liquid crystalline polymers can be found in the *Chemical Review* paper.^[4]

Aoki *et al.*^[23] have examined the correlation between the ability to control

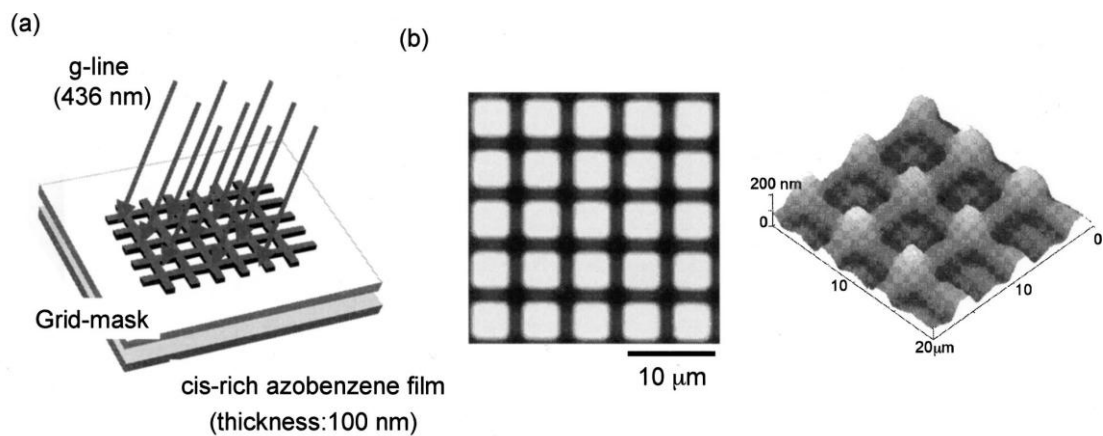


Figure 1-3 SRG inscribed on a liquid crystalline polymer by Zettsu.^[13]

a. Schematic illustration of the irradiation through a photomask with nonpolarized incoherent light

b. Photograph of a grid type photomask (left) and an AFM image of the resulting relief structure (right) after irradiation with 436 nm light from a mercury lamp (4 mW/cm² for 30 s).

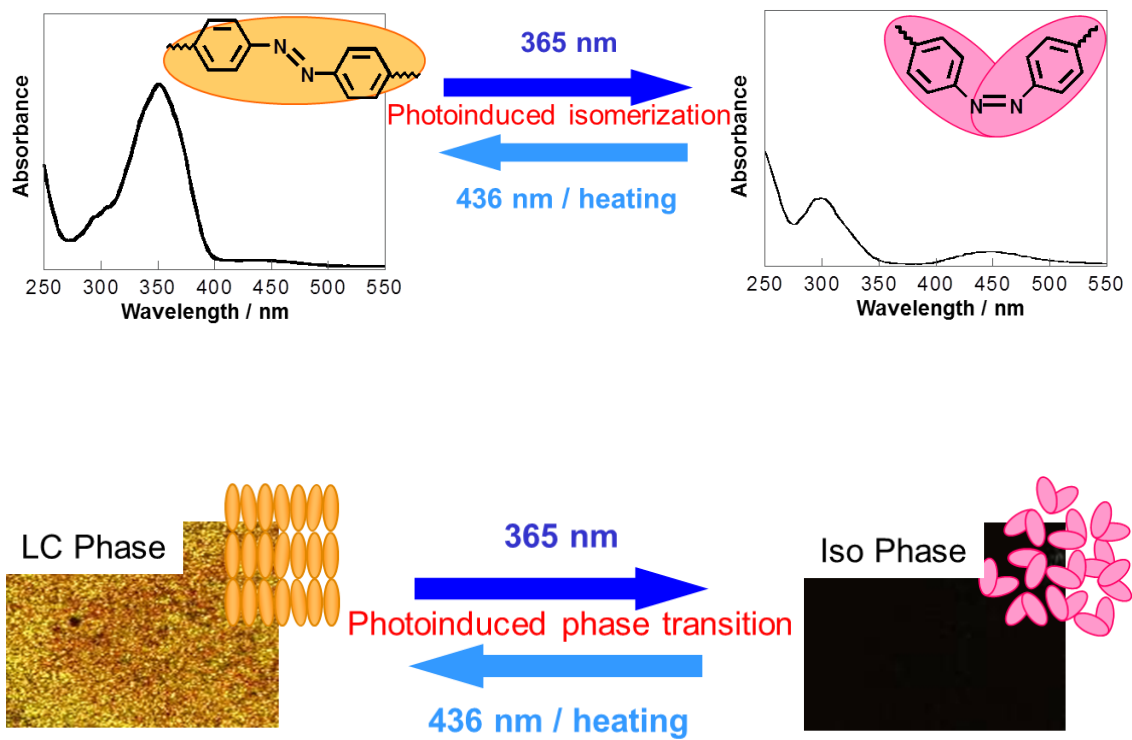
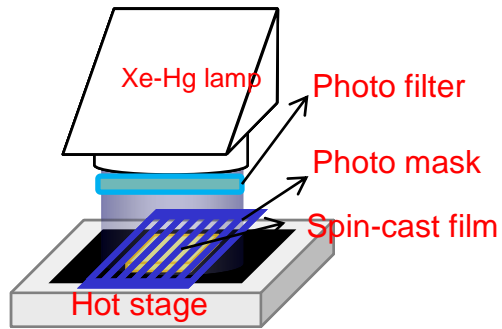


Figure 1-4 phase transition of Azo liquid crystalline polymer.

NLC alignment and wetting properties of outmost photoactive monolayers through Zisman plots method. The level of photoisomerization and surface free energy of command layer are not a sufficient criterion to cause the contrasting alignment behavior. Oh *et al.*^[24] has argued the most significant factor to induce the NLC alignment alternations. They prepared mixed monolayers formed by co-adsorption of two O-octacarboxymethylated calyx[4]resorcinarenes (CRA-CMs) with either perfluorooctyl- or octylazobenzene units. The authors claim that the morphology at molecular level and/or fluidity of the monolayer surfaces of CRA-CMs, which is deduced from the contact angle hysteresis of anisotropic liquids for the surface, is the most significant factor to cause the photo-tunable NLC alignment.

Ichimura *et al.*^[25] have demonstrated an exciting application of these kinds of phenomena, physical migrations of an olive oil droplet using light. When the azobenzene isomerizes, a gradient the surface free energy is produced, and this actually moves the oil drop at a millimeter scale.

In our lab, a family of soft liquid crystalline Az polymers applicable for SRG formation were developed. **(Figure 1-3, Figure 1-4)**^[10, 26-31] The use of soft liquid crystalline Az polymer allowed marked enhancement in the SRG formation upon patterned irradiation. The photon dose for the completion of migration is approximately 10^3 fold lower than that of widely reported amorphous and liquid crystalline polymers. From the knowledge obtained by our previous investigations, the mechanism of the SRG formation in this system could be assumed as follow. The patterned visible irradiation gives rise to the spatial distributions of the trans-rich and cis-rich regions. The film material starts to move from the trans-rich smectic liquid crystalline regions to cis-rich isotropic ones, which is possibly initiated by the disparities of the viscosity and sharp gradient of surface tension at the boundary

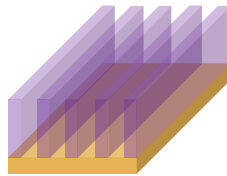


azobenzene containing liquid crystalline film



LC phase (Trans)

Photo-mask patterned **UV**



Dark : LC phase
Bright : Iso. phase

Dark
To bright



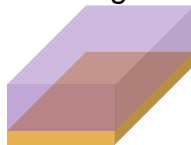
mass migration
LC to Iso phase

azobenzene containing liquid crystalline film



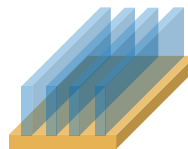
LC phase (Trans)

Homogenous UV



Iso. Phase (Cis-rich)

Photo-mask patterned **visible light**



bright : LC phase
dark : Iso. phase

bright
to dark



mass migration
LC to Iso phase

Figure 1-5. Two ways for SRG formation

regions.^[31, 32]

The most commonly used two methods to form a SRG are shown in **Figure 1-5**. In case of the top one, spin-cast films are exposed to patterned light beam directly. The light is generated from a Xe-Hg lamp source then passed through a UV filter (365nm) followed by a photo mask. A hot stage is set beneath the film to control the temperature. It is called a UV-inscription. In contrast, for the lower one, which is called Vis-inscription, two things are different from the upper one. First, before SRG formation the film is exposed to homogeneous UV light. Second, during SRG formation, the photo filter is Vis (463nm) filter. But one thing in common is that in both cases, only LC phase polymers moves toward isotropic phase polymers to form SRG.

1.2.4 Limitation of current SRGs

Due to the high sensitivity, the resulted relief pattern is not stable at high temperatures. But, the shape stability and durability at higher temperatures are of great demand in photonic applications such as waveguide couplers and aligning layers for liquid crystals. To solve this issue, some research groups have adopted various amorphous azobenzene polymers with high glass transition temperatures (T_g) such as azocarbazole-based polyimide, polyurethane containing V-shaped bisazo unit, and maleimide-based polymer. However, use of high- T_g polymers leads to significant reductions in the efficiency of the mass transport; the requirement for typical total photon dose reaches a level of a few hundred $J\ cm^{-2}$.^[10, 26-32]

There are basically two strategies to improve the stability of an inscribed relief structure, that is, use of high- T_g polymers and post-cross-linking. It has been recognized that the shape stability of the relief structure is strongly associated with the

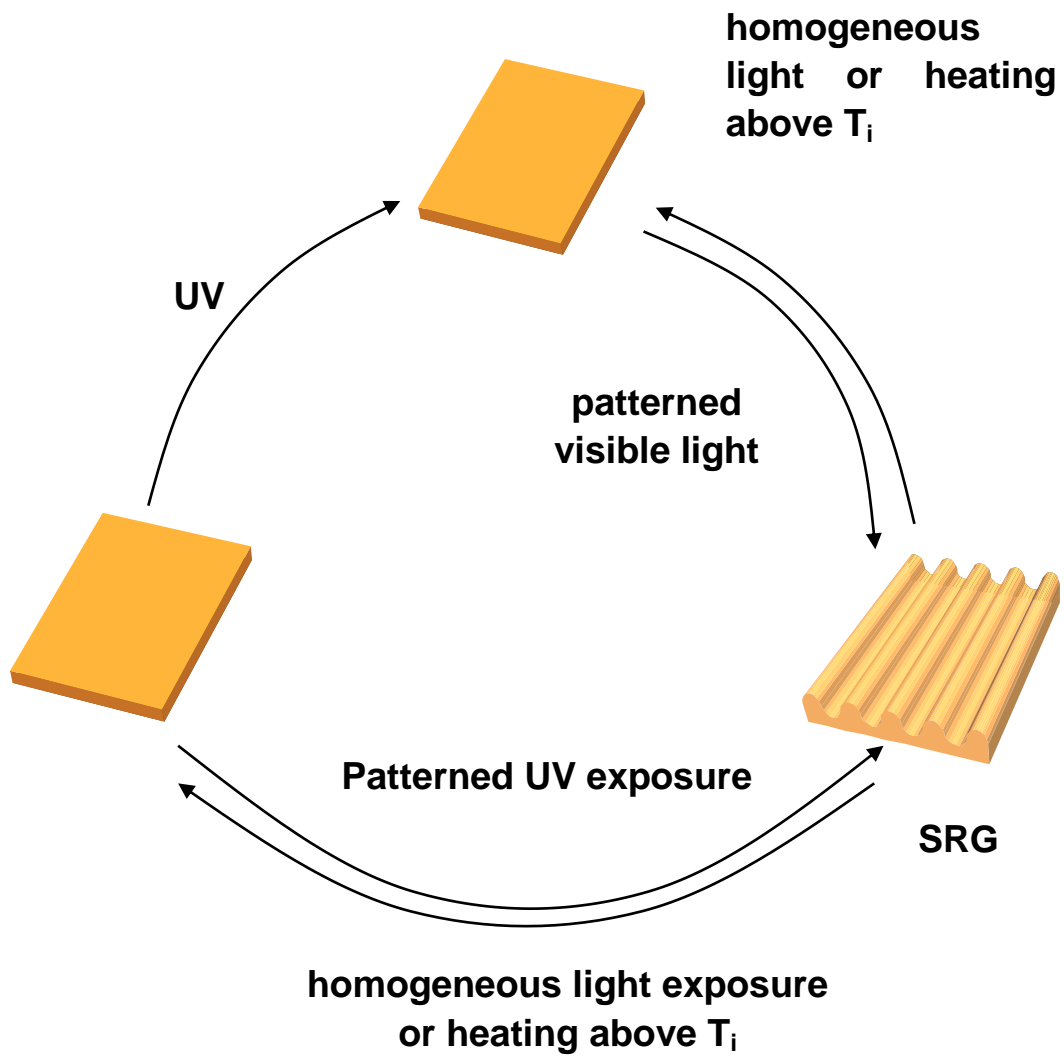


Figure 1-5 SRG formation and erasing of azobenzene containing liquid crystalline polymer film

rigidity of the polymer main chain.^{[33][34][35]} Some research groups have shown that use of high-T_g polymers is effective in improving the shape stability. Kimura^[36] and Takase^[37] have independently proposed photo-crosslinkable Az polymers as another strategy for shape stability. The thermal stability was also considerably enhanced with this method. However, the above two approaches pose additional disadvantages. High-T_g polymers require exposure to vast amounts of energy to promote the mass migration, and photo-cross-linking of the polymer film leads to photobleaching of the functional Az units.

1.2.5 Application of SRG

Since the initial report, the ease of inscription of SRG and their stability have pronounced a huge amount of proposed applications. The most obvious application is their use in one-step holographic image storage. It is possible to inscribe more than one hologram on same film surface by rotating the film at a desired angle. Natanshon *et al*^[38] have demonstrated that eight holograms are recorded on a single spot, but this is obviously not the limit. Other very interesting possible photonic applications including waveguide, liquid crystal alignment and so forth have been proposed.

1.3 Purpose of this research

The purpose of this work is to solve the drawbacks of the current SRG systems and propose new strategy introduction of hierarchical morphology in the liquid crystalline SRG forming materials by tuning the mobility of the material. The former aim would be attained by post-crosslinking of the material, and for the latter case, in contrast, more dynamic motions are added in the migrating process.

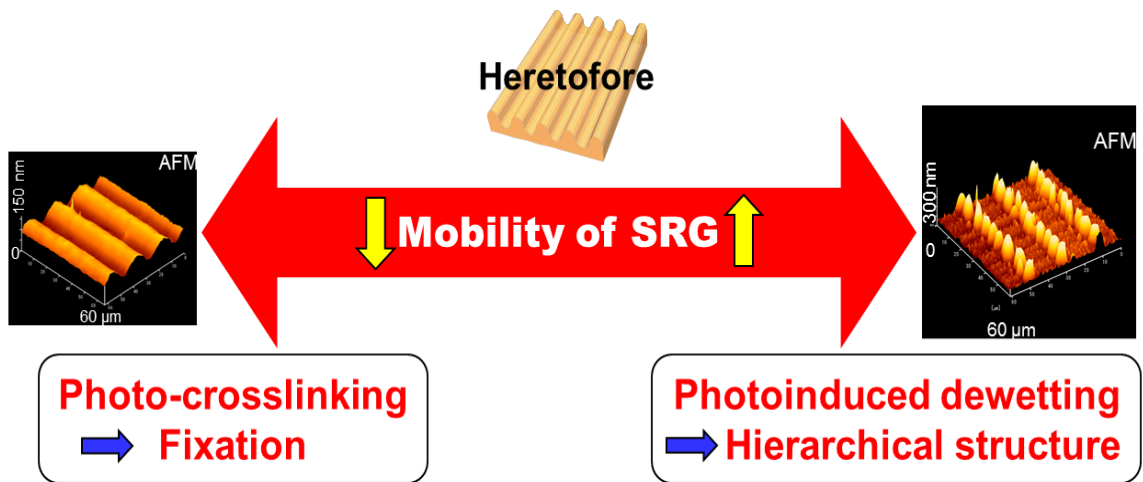


Figure 1-6 Two opposite ways on the research work of SRG.

As is shown in **Figure 1-6**, the current research of SRG focused mainly on the modification of the mobility of SRG material, either to decrease or increase it. In this thesis, the mobility of azobenzene derivatives will be altered in both directions. When increased the mobility, the SRG can be formed easier, while decreased, that can be removed hardly.

In Chapter 2, a new method for the purpose of decreasing this mobility will be displayed, which is called photoinduced crosslinking. The stability of SRG pattern will be strongly improved by this process.

Chapter 3 will involve a new concept for the increasing of thin film mobility, which will be used in to the SRG process in lateral experiments. This concept is called photoinduced dewetting. In this chapter, it will be shown that this procedure has a remarkable improvement in the mobility of thin films.

Chapter 4 showed the combination of SRG inscription and photoinduced dewetting. Such hybrid system played unexpected new improvements in photo science. With a remarkable improvement in the mobility of azobenzene dendrimers, a series of new SRG patterns will be displayed in this chapter.

References

1. A. Noble, *Annalen der Chemie und Pharmacie*, (1856), 98, 253
2. H. E. Bigelow, D. B. Robinson, *Orga. Syn.*, (1995), 3, 103
3. T. Todorov, L. Nikolova, N. Tomova, *Appl. Opt.* (1984), 23, 4309
4. K. Ichimura, *Chem. Rev.* (2000), 100, 1847
5. S. Tazuke, S. Kurihara, T. Ikeda, *Chemistry Letters*. (1987), 911
6. N. Tamaoki, *Adv. Mater.* (2001), 13, 1135
7. S. Pieraccini, S. Masiero, G. P. Spada, G. Gottarelli, *Chem. Commun.* (2003), 598
8. P. Rochon, E. Batalla, A. Natansohn, *Appl. Phys. Lett.*, (1995), 66, 136
9. D. Kim, S. Tripathy, L. Li, J. Kumar, *Appl. Phys. Lett.* (1995), 66, 1166
10. N. Zettsu, T. Fukuda, H. Matsuda, T. Seki, *Appl. Phys. Lett.* (2003), 83, 4960

11. S. Bian, J. M. Williams, D. Y. Kim, L. Li, S. Balasubramanian, J. Kumar, S. K. Tripathy, *J. Appl. Phys.* (1999), *86*, 4498
12. N. K. Viswanathan, S. Balasubramanian, L. Li,; S. K. Tripathy, J. Kumar, *Jpn. J. Appl. Phys.* (1999), *38*, 5928
13. K. Ichimura, Y. Suzuki, T. Seki, A. Hosoki, K. Aoki, *Langmuir.* (1988), *4*, 1214
14. K. Kawanishi, T. Tamaki, M. Sakuragi, T. Seki, Y. Suzuki, K. Ichimura, *Langmuir.*(1992), *8*, 2601
15. K. Ichimura, Y. Hayashi, N. Ishizuki, *Chem. Lett.* (1992), *5*, 1063
16. K. Ichimura, Y. Hayashi, H. Akiyama, T. Ikeda, N. Ishizuki, *Appl. Phys. Lett.* (1993), *63*, 449
17. K. Kawanishi, T. Tamaki, K. Ichimura, *Polym. Mater. Sci. Eng.* (1992), *66*, 263
18. M. Kidowaki, T. Fujiwara, K. Ichimura, *Chem. Lett.* (1999), 643
19. C. Ruslim, K. Ichimura, *Adv. Mater.* (2001), *13*, 641
20. K. Ichimura, S. Furumi, S. Morino, M. Kidowaki, M. Nalagawa, M. Ogawa, Y. Nishimura, *Adv. Mater.* (2000), *12*, 950
21. K. Ichimura, M. Momose, T. Fujiwara, *Chem. Lett.* (2000), *13*, 1022
22. C. Ruslim, M. Hashimoto, D. Matsunaga, T. Tamaki, K. Ichimura, *Langmuir.* (2004), *20*, 95
23. K. Aoki, Y. Kawanishi, T. Seki, M. Sakuragi, T. Tamaki, K. Ichimura, *Liq. Cryst.*(1995), *19*, 119
24. S. K. Oh, M. Nakagawa, K. Ichimura, *J. Mater. Chem.*(2001), *11*, 1563
25. K. Ichimura, S. K. Oh, M. Nakagawa, *Science.*(2002), *288*, 1624
26. T. Ubukata, T. Seki, K. Ichimura, *Adv. Mater.*(2000), *12*, 1675
27. T. Ubukata, T. Higuchi, N. Zettsu, T. Seki, M. Hara, *Colloids & Surf. A*, (2005), *123*, 257
28. T. Ubukata, M. Hara, K. Ichimura, T. Seki, *Adv. Mater.* (2004), *16*, 220
29. N. Zettsu, T. Ubukata, T. Seki, K. Ichimura, *Adv. Mater.* (2001), *13*, 1693
30. N. Zettsu, T. Seki, *Macromolecules.* (2004), *37*, 8692
31. N. Zettsu, T. Ogasawara, R. Arakawa, S. Nagano, T. Ubukata, T. Seki, *Macromolecules.* (2007), *40*, 4607
32. T. Seki, *Curr. Opin. Solid State Mater. Sci.* (2007), *10*, 241
33. T. Lee, D. Kim, X. L. Jiang, L. Li, J. Kumar, S. Tripathy, *J. Polym. Sci., Part A.* (1998), *36*, 283
34. Y. Wu, A. Natansohn, P. Rochon, *Macromolecules.* (2001), *34*, 7822
35. T. Fukuda, H. Matsuda, T. Shiraga, T. Kimura, M. Kato, N. Viswanathan, J. Kumar, S. K. Tripathy, *Macromolecules.* (2000), *33*, 4220
36. T. Kimura, J. Y. Kim, T. Fukuda, H. Matsuda, *Macromol. Chem. Phys.* (2002), *203*, 2344

37. H. Takase, A. Natansohn, P. Rochon, *Polymer*. (2003), 44,7345

Chapter 2

Photo-crosslinkable Liquid-crystalline azo-polymer for Surface Relief Gratings and Persistent Fixation

2.1 Introduction

It is known that SRG structures can be erased by homogeneous light irradiation. There are basically two strategies for improved stability of the inscribed relief structure, that is, use of high- T_g polymers and post-cross-linking. It has been recognized that the shape stability of the relief structure is strongly associated with the rigidity of the polymer main chain. Some research groups have shown that use of high- T_g polymers is effective in improving the shape stability. Kimura et al.^[18] has proposed photocross-linkable Az polymers as another strategy for shape stability. The thermal stability was also considerably enhanced with this method. However, the above two approaches pose additional disadvantages. High- T_g polymers require exposure to vast amounts of energy to promote the mass migration, and photo-cross-linking of the polymer film leads to photobleaching of the functional Az units.

Crosslinking is the process of chemically joining two molecules by a covalent bond. Cross-linking reagents contain reactive ends to specific functional groups (primary amines, sulfhydryls, etc.) on proteins or other molecules. Several chemical groups that may be targets for reactions in proteins and peptides are readily available, allowing them to be easily conjugated and studied using cross-linking

methods. Cross-linkers also are commonly used to modify nucleic acids, drugs, solid surfaces and other molecules.

2.1.1 Chemical crosslinking

In contrast, here I would like to give a brief introduction of the chemical crosslinking purchased by Zettsu *et al.*^[16-19], in the purpose of fixing a SRG structure. As shown in **Figure 2-1**. by involving this system, his SRG patterns were able to stay up to 250°C, which is times higher than the SRG structures without this fixation (100°C). However, this process has its own disadvantage. After all, it is a wet process. Also, it is tedious in handling and requires for a long period of reacting time (6 hours).

2.1.2 Photo-initiated crosslinking

Photo-initiated crosslinking is often used as it is usually rapid, effective, and well-controlled, and can be carried out at low temperatures.^[39-41] Among various photo-crosslinkable groups, cinnamic group has attracted particular attention.^[3-5] Cinnamic group either in the backbone or side chain of a polymer can easily undergo a crosslinking reaction through [2 + 2] cycloaddition of the carbon-carbon double bonds upon irradiation with UV light.^[1,2]

The photo functionality of a cinnamate in a polymer arises from 2+2 dimerization leading the polymer chain to insolubilization, which is due to the formation of crosslinking bonds resulted in cyclobutane unites. (**Figure 2-2**)

In year 2002, Kimura had a publishing in which photo-crosslinking after SRG inscription was reported to be achieved. Both azobenzene and cinnamate were acting as side chains in a polymer abbreviated as PMPDC x-y. For SRG structure of PMPDC 21-18, in which 21 and 18 are related to mole percent of azobenzene and

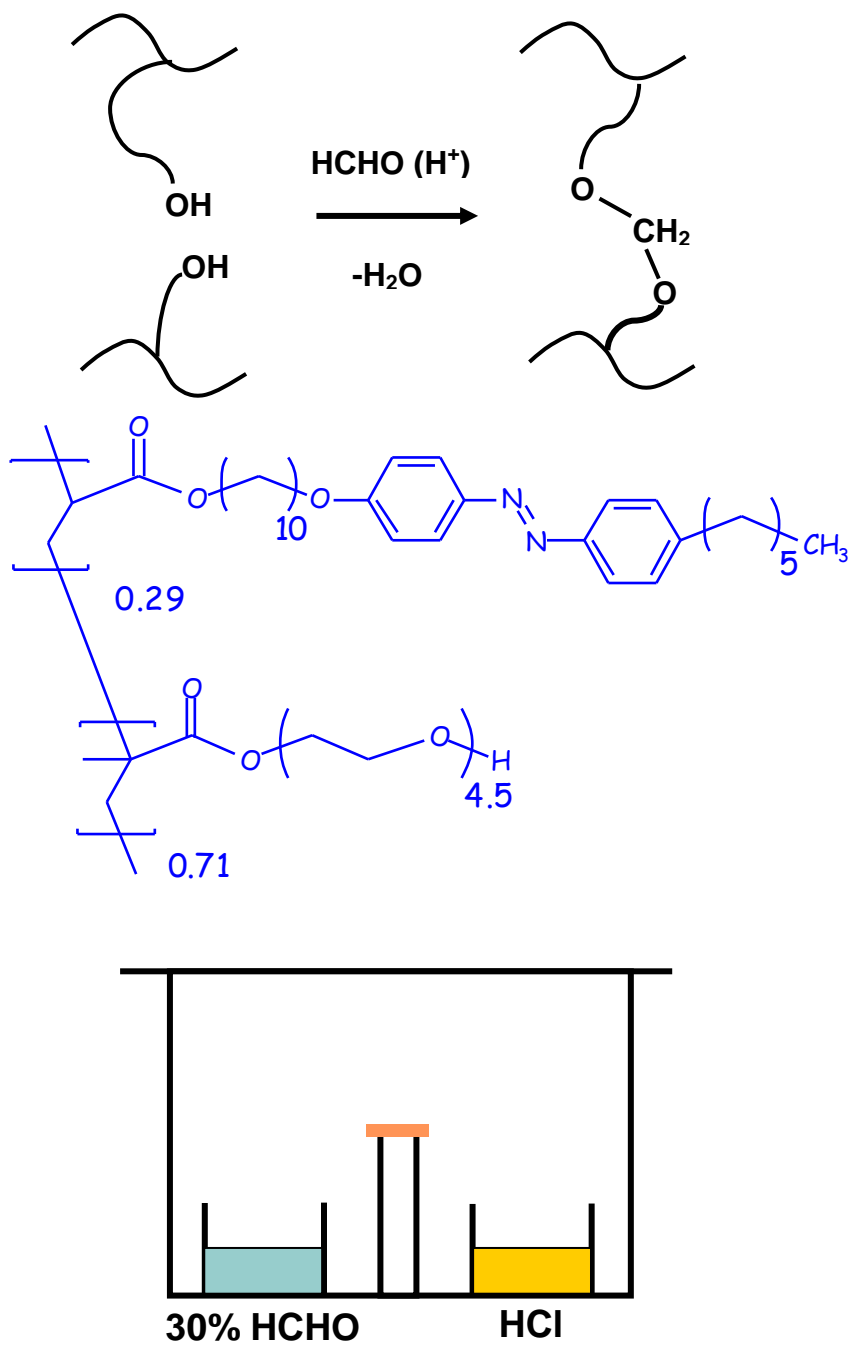


Figure 2-1 A chemical crosslinking polymer and its system for the fixation of SRG pattern.

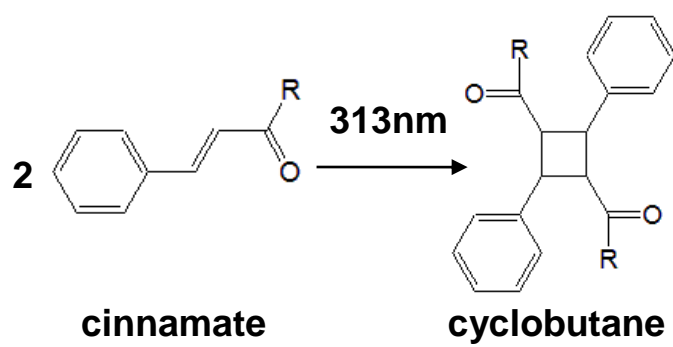


Figure 2-2 2+2 dimerization of cinnamate.

cinnamate side chain, the temperature dependence before and after photo-crosslinking was discussed. Later the result of their experiment will be introduced again in contrast with our result, to clarify the efficiency of photo-crosslinking process.

2.2 Experimental

The chemical structure of the polymer used in this study was shown in **Figure 2-3**. The copolymers containing both an azobenzene unit and an oligo(ethylene oxide) chain were synthesized by free radical random copolymerization of acrylate or methacrylate monomers. The detailed information on synthetic procedures was described below.

All reagents, purchased from Aldrich Chemical, Kanto Chemical, or Tokyo Chemical Industry, were used without further purification. The reaction progress was monitored through thin layer chromatography (TLC) on silica gel (Merck, Kieselgel 60 F254).

2.2.1 Synthesis of 4-[(4'-pentyl)azo]phenol (5Az-OH)

4-[(4'-pentyl)azo]phenol (5Az-OH) was synthesized by diazo-coupling of 4-pentylaniline with phenol according to a conventional procedure. 4-pentylaniline (30 mmol) was dissolved in a mixture of concentrated hydrochloric acid and water. After cooling, the aniline was diazotized by dropping a solution of NaNO₂ (60 mmol) in water at 0-5 °C. Addition of diazotized solution to a solution of phenol (60 mmol), NaOH, Na₂CO₃ in water led to proceeding of the diazo-coupling reaction. After neutralization and subsequent filtration, the precipitate was recrystallized from hexane. Recrystallization gave pure 6AzOH as yellow powder in an 87% yield.

¹H-NMR(400MHz, CDCl₃, TMS) [ppm]: 0.89 (3H, t, CH₃-), 1.31-1.68 (6H, m,

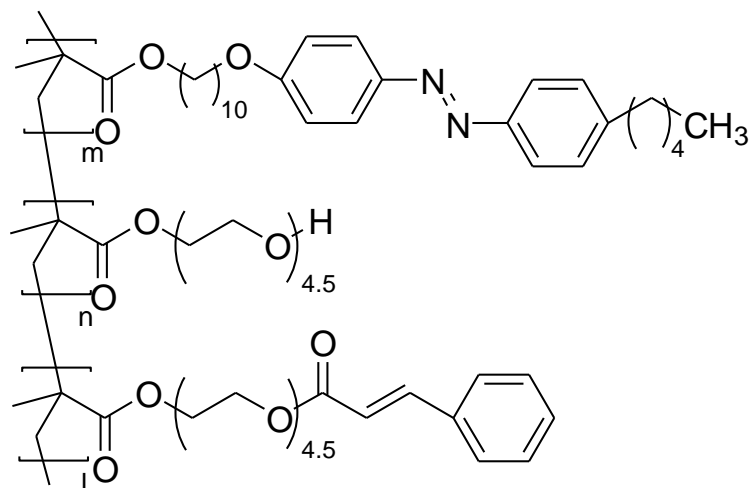


Figure 2-3 Designed polymer for SRG inscription and photo-crosslinking.

-CH₂-), 2.67 (2H, t, -CH₂-Ph), 5.13 (1H, s, Ar-OH), 6.94 (2H, d, Ar-H), 7.27 (2H, d, Ar-H), 7.76-7.88 (4H, q, Ar-H).

2.2.2 Synthesis of 4-(10-hydroxydecyl)-4'-pentylazobenzene (5Az10-OH)

4-[(4'-pentyl)azo]phenol (5Az-OH) was converted to 4-(10-hydroxydecyl)-4'-pentylazobenzene (5Az10-OH) by Williamson's esterification reaction. To a stirred dried acetone solution (20 ml) dissolved 5AzOH (30 mmol), powdered potassium carbonate (8 mmol), and potassium iodide as a catalyst was added a dried acetone solution dissolved 10-bromododecanol (6 mmol) in dried acetone. The mixture was stirred at refluxing temperature for 20h. After removing a precipitate, a filtrate was concentrated to give a solid residue, which was purified by recrystallization from hexane at least twice to give a solid residue, which was purified by Recrystallization from hexane at least twice to give a yellow powder in a yield of 91%.

¹H-NMR(400MHz, CDCl₃, TMS) [ppm]: 0.91 (3H, t, CH₃-), 1.19-1.83 (6H, m, -CH₂-), 2.65 (2H, t, -CH₂-Ph), 3.67 (2H, t, -CH₂-O-), 4.05 (2H, t, -O-CH₂-), 6.99 (2H, d, Ar-H), 7.27 (2H, d, Ar-H), 7.77- 7.89 (4H, q, Ar-H).

2.2.3 Synthesis of

4-(10-methacryloyloxydecyloxy)-4'-pentylazobenzene (5Az10Me)

The mixture of 5Az10-OH (5 mmol) and triethylamine (10 mmol) in dried tetrahydrofuran (THF) was added to a solution of acryloyl chloride (10 mmol) in THF under a nitrogen atmosphere, and was stirred at room temperature for 5h. The resulting raw product was washed in water for several times and dried over

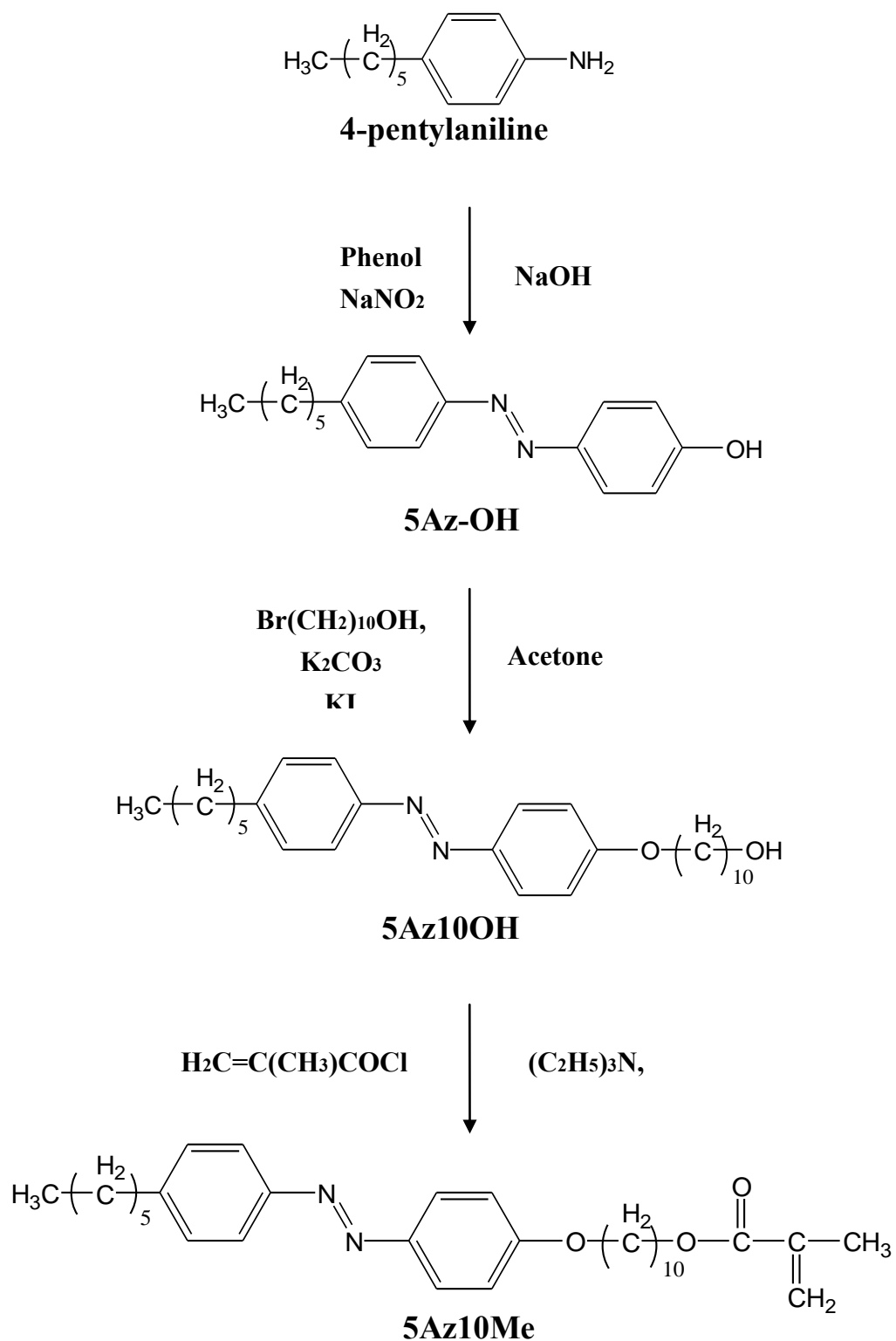


Figure 2-4 Synthesis of 5Az10Me

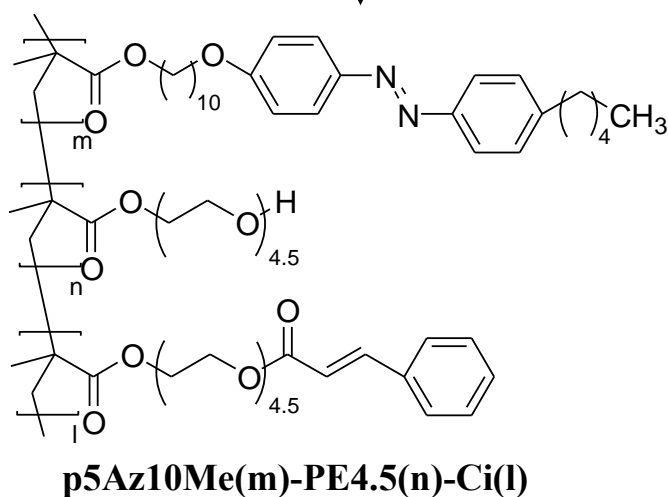
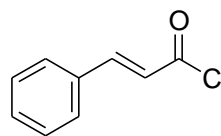
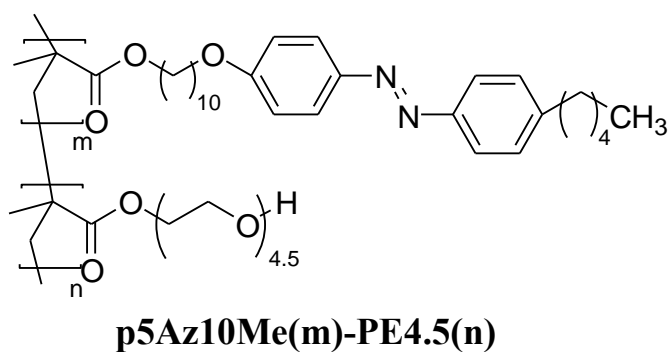
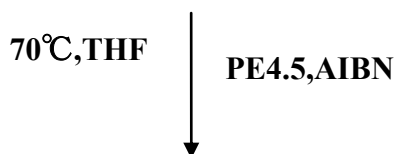
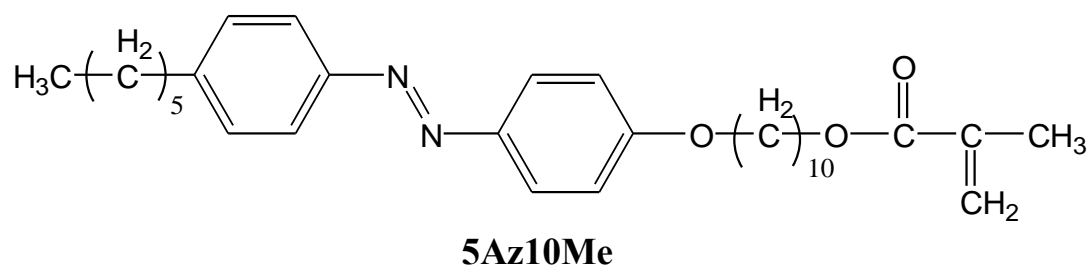


Figure 2-5 synthesis of p5Az10Me(m)-PE4.5(n)-Ci(l)

magnesium sulfate. After removing the solvent, the solid residue was recrystallized twice from methanol to give pure 4-(10-methacryloyloxydecyloxy)-4'-pentylazobenzene (5Az10Me) as a yellow powder in a 87% yield.

¹H-NMR (400MHz, CDCl₃, TMS) [ppm]: 0.89 (3H, t, CH₃-), 1.33-1.94 (25H, m, -CH₂-; CH₃-), 2.67 (2H, t, -CH₂-Ph), 4.00 (2H, t, CH₂-O-), 4.16 (2H, t, -O-CH₂), 5.54 (1H, d, Vinyl-H), 6.09 (1H, d, Vinyl-H), 6.97 (2H, d, Ar-H), 7.27 (2H, d, Ar-H), 7.77-7.89 (4H, q, Ar-H).

2.2.4 Polymerization of p5Az10Me-PE4.5

The azo containing polymer was synthesized in dry-THF (5 ml) solution under nitrogen circumstance, using AIBN (0.0392 mmol) as an initiator via free radical polymerization of the 5Az10Me monomer (0.245 mmol) and PE200 (0.49 mmol), another methacrylate monomer containing an oligo (ethylene oxide unit) chain. This polymer was abbreviated as p5Az10Me-PE4.5. The reaction media was heated at 70 °C for 6h, cooled to room temperature, and then poured in to a vigorously stirred hexane for reprecipitation. The resulting polymer was collected by centrifugation. The orange solid product was dried in vacuum. The reaction yield was 70%.

2.2.5 Synthesis of p5Az10Me-PE4.5-Ci

Finally, using p5Az10Me-PE4.5 (0.223 mmol) and cinnamoyl chloride (0.116 mmol) as reactants, dry-THF (4 ml) as a solvent a polymer involving both azobenzene and cinnamate as side chains was synthesized by stirring the mixture at room temperature for 5 h. Reprecipitation was done in a mixture solvent of 98.5%

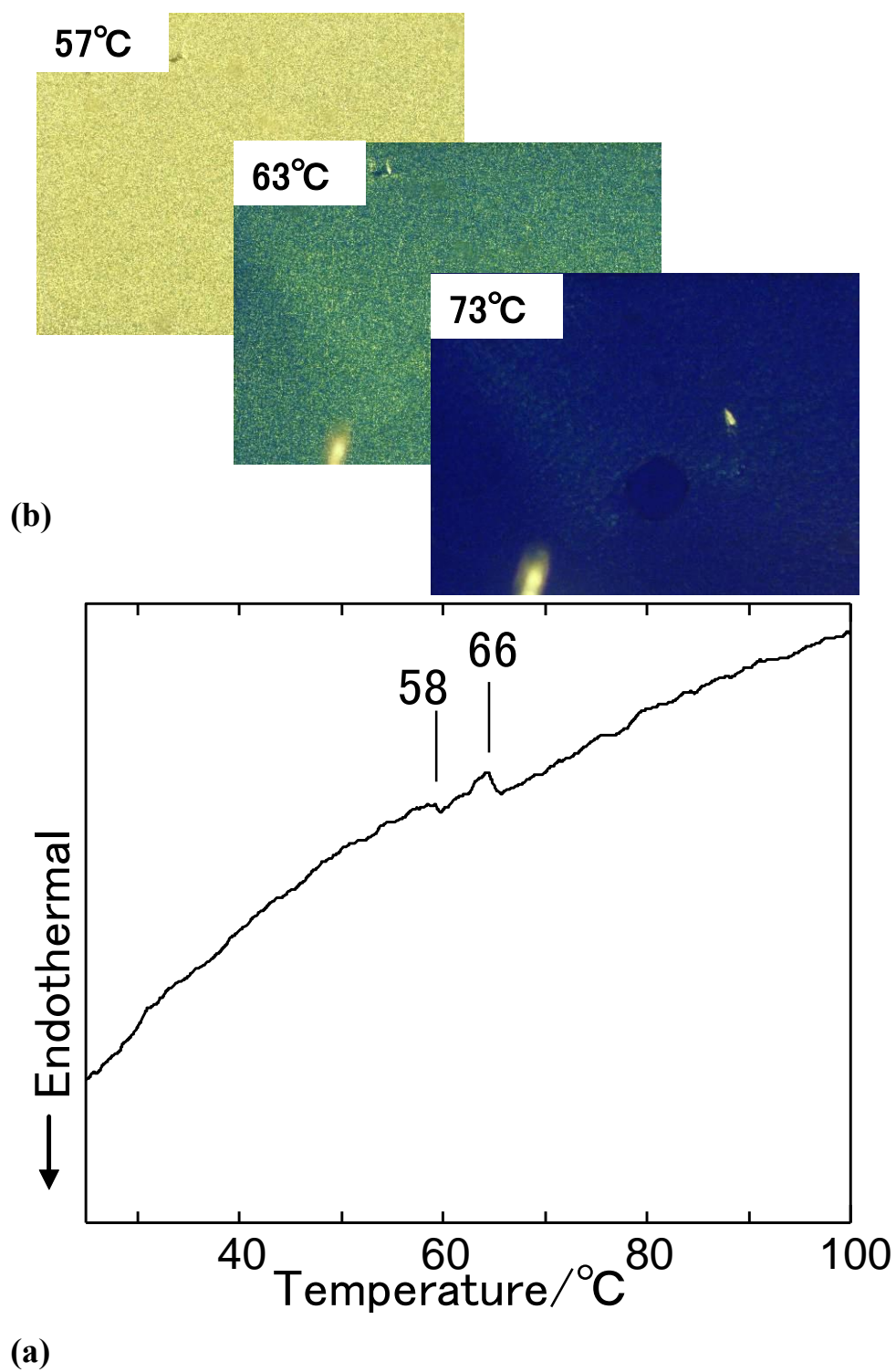


Figure 2-6 Thermal analysis of p5Az10Me(38)-PE4.5(48)-Ci(14)

(a) DSC, (b) POM

hexane and 1.5% chloroform. After dried in vacuum, the product was observed as a sticky orange solid in a yield of 80%. This product was abbreviated as p5Az10Me-PE4.5-Ci, and the copolymerization ratio (m, n and l) was determined by ¹H-NMR as described in the section of Result and Discussion.

2.2.6 Gel permeation chromatography (GPC) measurements

Molecular mass data for the polymer was achieved by gel permeation chromatography (Shodex Technology). According to GPC data, it can be identified that both weight-average molecular weight and number average molecular weight of our product. In this case, THF as a solvent for GPC measurement were used.

The final product showed an weight-average molecular weight (M_w) of 1.51×10^4 and a number average molecular weight (M_n) of 1.18×10^4 ($M_w/M_n = 1.45$).

2.2.7 DSC measurements

Differential scanning calorimetry (DSC) was undertaken with a DSC 6200 (Seiko Instruments Inc.). This is a thermo analytical technique in which the difference in the amount of heat required to increase the temperature of a sample and reference are measured as a function of temperature. Both the sample and reference are maintained at nearly the same temperature throughout the experiment. Generally, the temperature program for a DSC analysis is designed such that the sample holder temperature increases linearly as a function of time. The reference sample should have a well-defined heat capacity over the range of temperatures to be scanned. In this case, air was used as a reference. Sample weight was around 5mg. By measuring at the temperature range of 20 to 100°C for 2 times. Datas of the 2nd decreasing(3°C/min) was collected (**Figure 2-6**). Two peaks were observed, one at 58°C, while another at

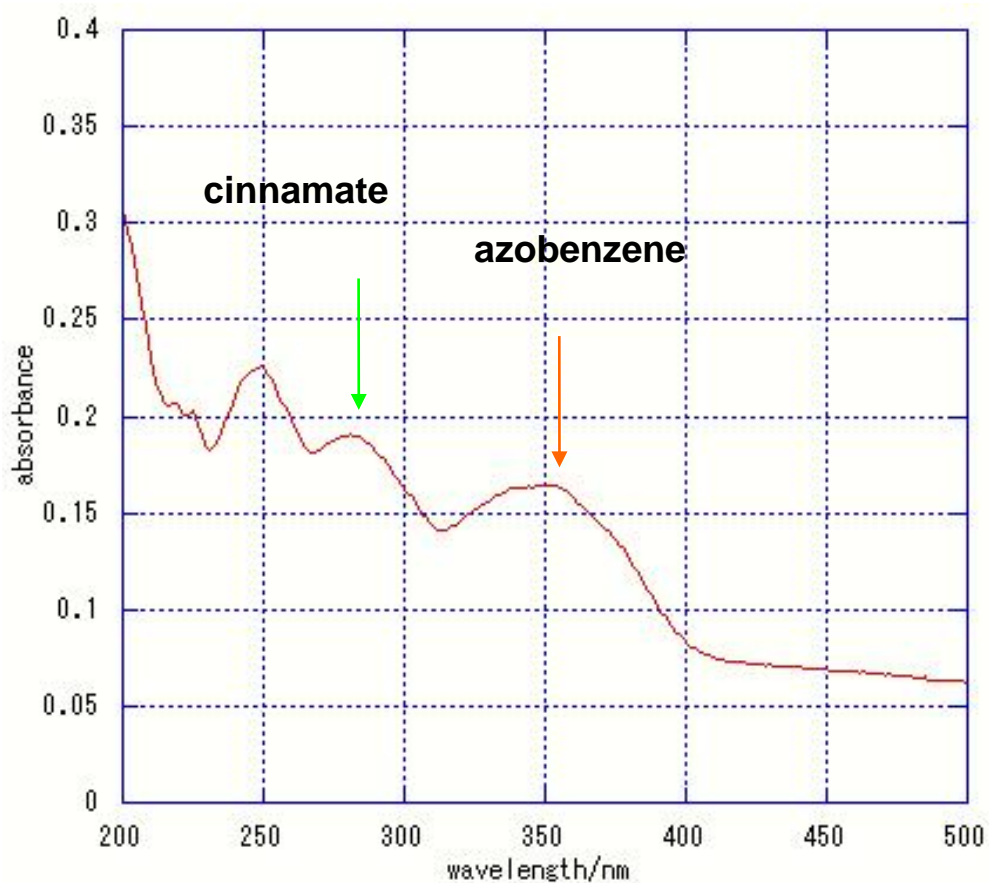


Figure 2-7 UV absorbance of synthesized polymer p5Az10Me-PE4.5-Ci

66°C, indicating 2 phase transition temperatures.

2.2.8 Polarized optical microscopic (POM) measurements

The polarized optical microscopic (POM) observations were made using a BX51 (Olympus Technology). A polarizing microscope has a pair of polars (polarizing devices) in the optical train. The first polar (polarizer) defines the initial plane of polarization for light entering the microscope and is located between the illuminator and the condenser. The other polar (analyzer) is placed between the objective and the ocular tube and defines the plane of polarization of the light reaching the ocular.

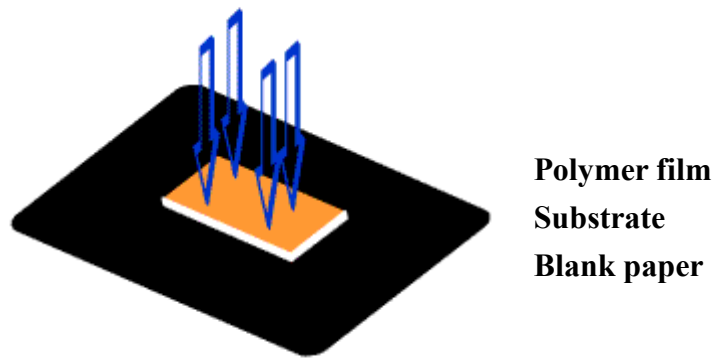
A POM image at 63 °C clearly exhibited a birefringence, indicating the liquid crystalline phase. On the other hand, the birefringence disappeared corresponding to the endothermal transition, and the POM image became fully dark at 73 °C. The above two kinds of thermal data indicate that the two characteristic transitions at 58 and 66 °C correspond to T_g and T_i , respectively.

2.2.9 UV-vis absorption spectra measurements

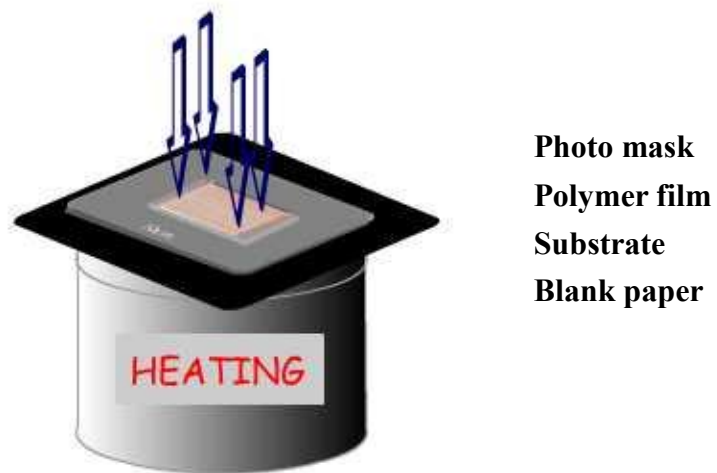
UV-vis absorption spectra were taken on an Agilent 8453 spectrophotometer (Agilent Technology). All at room temperature, using blank substrate as reference, sample films UV-vis absorption were measured.

As marked in **Figure 2-7**, the absorption peak at 280nm belongs to cinnamate side chain, while the peak at 350nm belongs to azobenzene side chain (trans).

2.2.10 Film fabrication



(a)



(b)

Figure 2-8 (a) scheme for pre-irradiation; (b) scheme for SRG inscription

Before the inscription of SRG structure, polymer thin films were prepared by spin-coating method. The quartz substrates were formerly cleaned by sequential ultrasonic treatments for 15min immersing in the following fluids, THF, saturated KOH/methanol, deionized water. After dried in air, films were remained on the surface of substrate. Polymer was dissolved into THF at a ratio of 2wt%. Then, on cleaned quartz substrates (1 cm×1.5 cm), films were fabricated by spin-coating this solution at 2000rpm for 30s. After that, films were dried in air for 10 minutes at room temperature. Film thickness was about 70nm as evaluated by atomic force microscope (AFM, Seiko Instruments: Nanopics 2100).

2.2.11 SRG formation

The mass migration requires a step of pre-exposure to UV light. (**Figure 2-8**) Without this procedure, SRG formation was barely observed at a certain intensity of exposure. Thus, the rapid SRG formation requires an initial cis-rich state, and should be driven by specially patterned cis-to-trans back photoisomerization via a photochemical phase transition from the isotropic liquid to the liquid crystal phase. So, the films were first exposed to homogenous UV light of 365 nm, which provides a cis-rich isomerization state in the whole area of the films.

Device used for this process was shown as below. Photo-mask of a 10 m line-and-space pattern was placed on top of the film. Then this film with the photo-mask on top was irradiated to light of 436 nm through the photo-mask at 50 °C.

The temperature was chosen Based on this polymer's T_g . according to our experience, SRG formation is more likely to be happening around T_g , which in this case was 58°C. Also SRG was inscribed at 45 and 55°C. In contract, it was noticed that the SRG inscribed at 50°C obtained the clearest pattern.

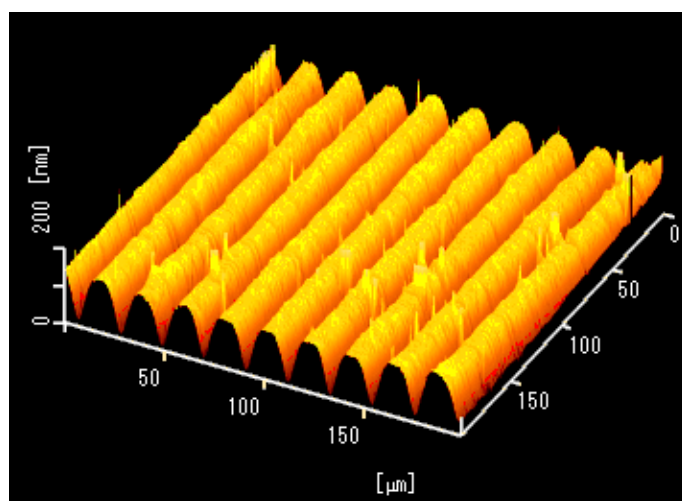
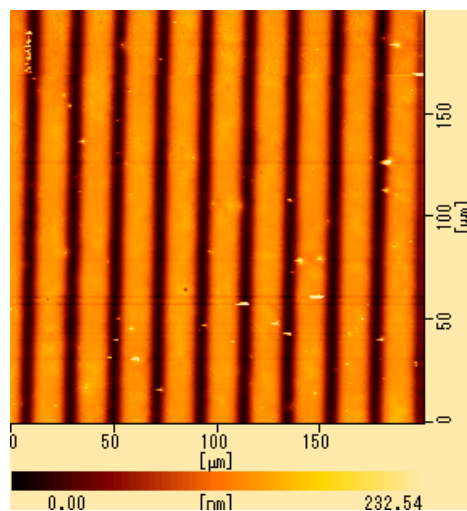


Figure 2-9 AFM image of inscribed relief gratings on a p5Az10Me-PE4.5-Ci film surface.

Generally, the variation of light intensity varies only the photo-chemical reaction rate. However, in molecular assembly systems, nonlinear phenomena can be involved with respect to the irradiation light intensity. In this contest, energy data needing for SRG formation, including the irradiation power and irradiation time, were optimized by repeating the irradiating processes at different conditions and comparing the SRG structures. By then, it was confirmed that optimized irradiation conditions for the SRG formation were as follows: pre-irradiation with 365 nm light: 10 mW cm⁻² exposure for 200 s (2 J cm⁻²) at room temperature, and subsequent patterned irradiation at 436 nm: 5mW cm⁻² for 200 s (1 J cm⁻²) at 50 °C. Both energy doses are much lower than those required for the UV-curable polymer previously reported.

2.2.12 AFM observation

This inscribed SRG pattern after these procedures observed by AFM is shown in **Figure 2-9**. The surface profile exhibited an regular undulated shape with a grating depth of 130 nm and a grating width of 20 μm. The top-to-top distance exactly corresponded to the mask patterns. Thus, the highest regions reached approximately the double of the initial film thickness, indicating the full mass transfer occurred during the optimized procedures.

2.3 results and discussion

2.3.1 UV-vis absorption during SRG formation

Changes in the UV absorption spectrum during the above process have been indicated in **Figure 2-9**. The initial film in the trans-Az state (solid line) showed the π - π^* absorption maximum at 347 nm. The absorption band around 280 nm is

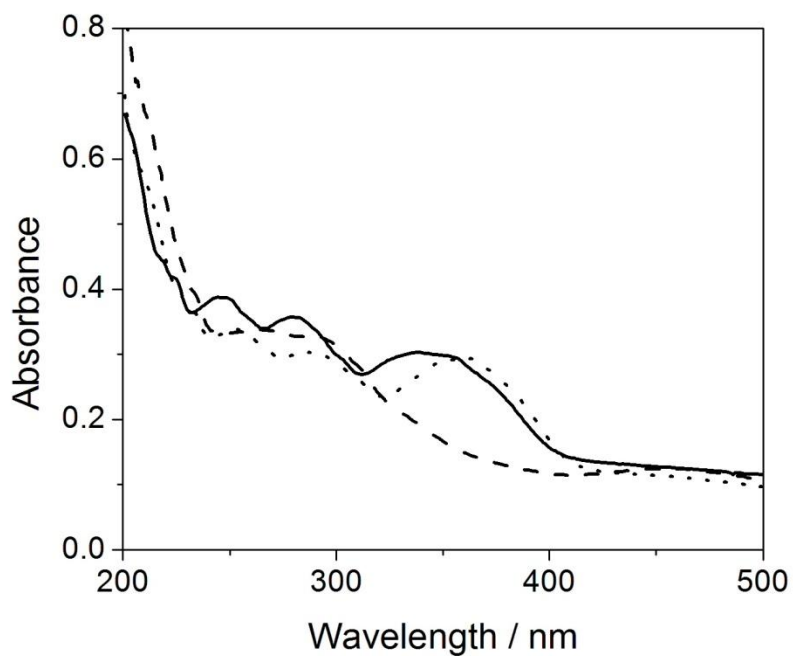


Figure 2-10 UV-vis absorption of sample film during SRG inscription process. Solid line for the original film; dashed line for the film irradiated with 365 nm UV; and dot line for the film subsequently exposed to 436 nm light.

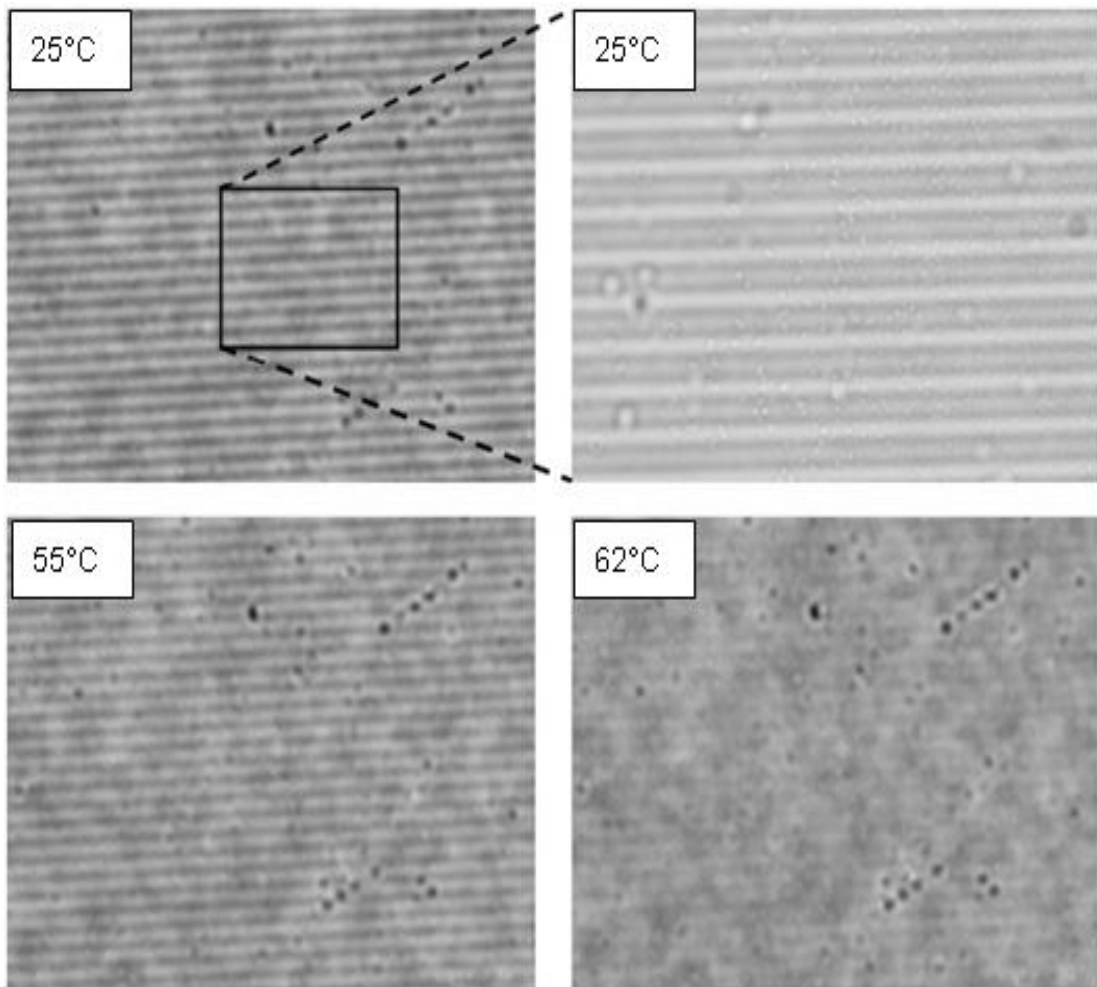


Figure 2-11 Optical microscope images taken while heating a SRG inscribed film from 25°C to 7°C in a rate of 2°C min⁻¹. The top-right image displays the magnified region for the top-left one.

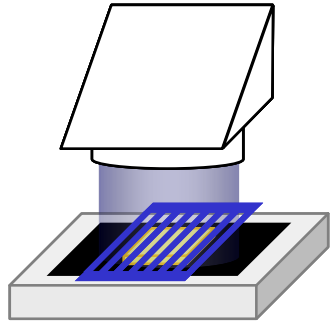
ascribed to the π - π^* absorption of cinnamoyl unit. By irradiation with 365 nm light the Az unit was efficiently isomerized to cis form (dashed line). After subsequent irradiation with 436 nm light, the Az unit was mostly reverted to the trans form (dotted line), but in this case the band peak of the π - π^* absorption was shifted to 361 nm, indicating the disruption of partial H aggregation in the initial film.

2.3.2 Light intensity comparing with former researches

In the experiment, 10 mW cm⁻² exposures for 200 s (2 J cm⁻²) as a pre-irradiation, followed by a 5mW cm⁻² for 200 s (1 J cm⁻²) for SRG inscription were used. Comparing to the former polymer produced by Zettsu in our lab, 40 mW cm⁻² for 20s (0.8 J cm⁻²) for pre-irradiation and 200 mW cm⁻² for 5s (1 J cm⁻²), the photon dose of this experiment is relatively high. It is suggested that this is caused of at least the following 2 reasons: 1) the polymer back bone is different, in this polymer, methacrylate was used as a main chain, while in Zettsu's case, ethacrylate was used. This change increased the rigid of our polymer, which leaded to a poor fluidity and result in a high energy cost for mass migration consquently; 2) the involving of cinnamate side chain also decreased the fluidity of product polymer and increased the energy cost. However, this photon dose is still relatively lower as the process was happened at liquid crystalline phase of the product polymer.

2.3.3 Thermal stability of SRG before crosslinking

During heating the SRG inscribed film from 25 to 70 °C at 2 °C min⁻¹, optical microscope observations were observed, as shown in **Figure 2-11**. Upon gradual heating, the SRG pattern started to collapse from 55 °C, and almost disappeared at

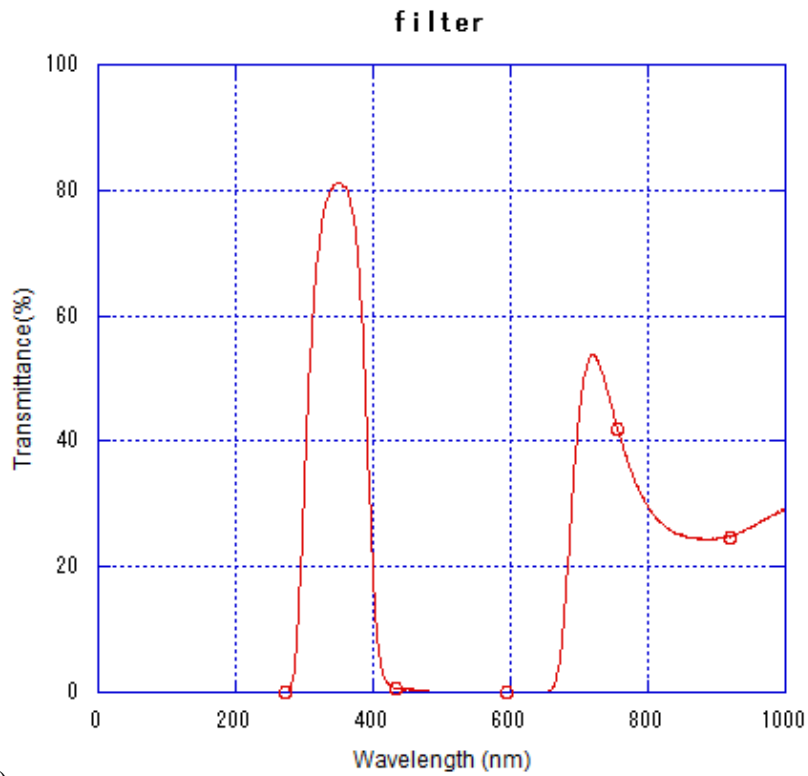


Visible light(436 nm)

5 mw cm⁻² x200s

50 °C

(a)



(b)

Figure 2-12 (a) Device of photo-crosslinking process; (b) Optical property of filters.

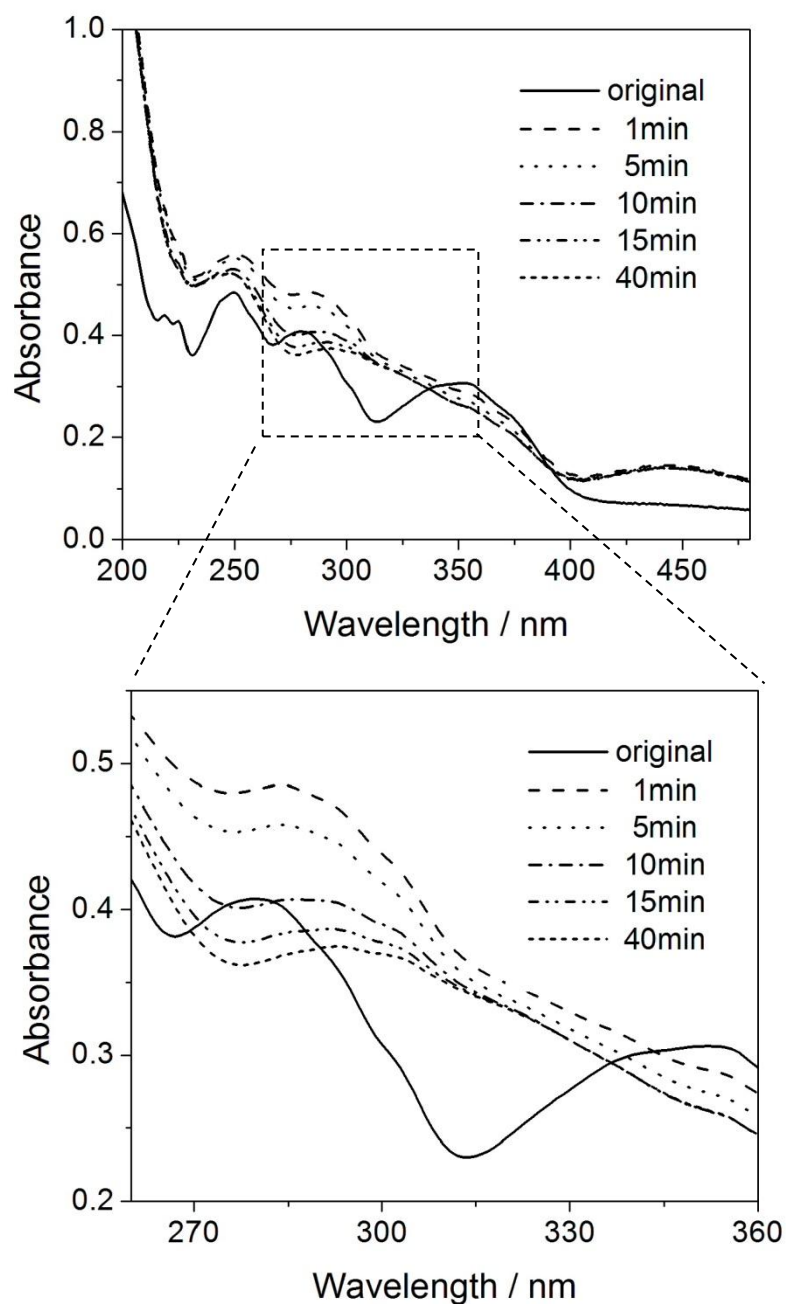


Figure 2-13 UV-vis absorption spectra of the copolymer film irradiated with UV at wavelengths ranging 300 – 400 nm at room temperature while changing the irradiation time from 1 to 40 min. The bottom figure displays the magnification of the enclosed region of upper one.

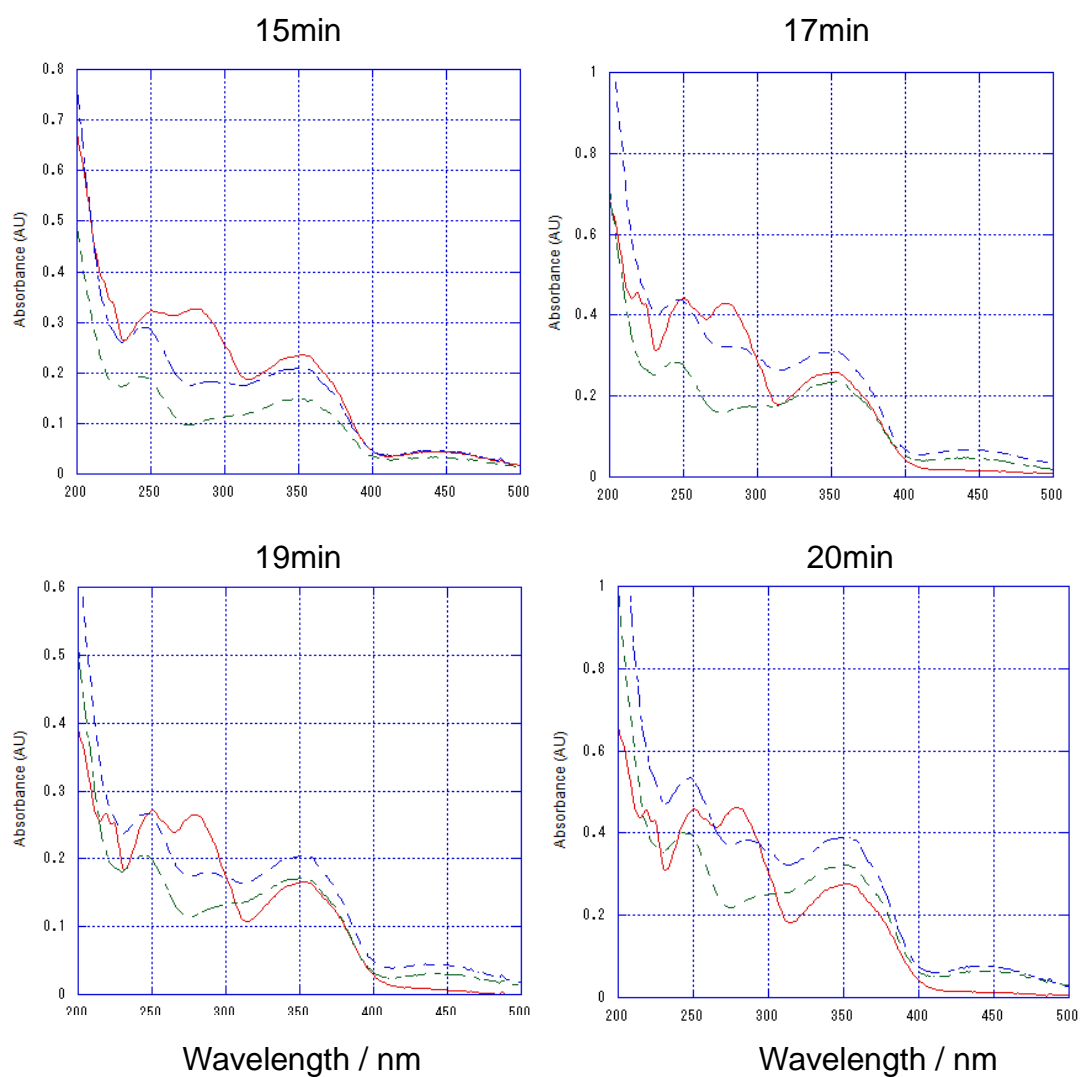


Figure 2-14 4 films being crosslinked for a series of time, then ruined in THF. UV absorption during this process was taken for comparing. Red line for original films; blue line for crosslinked films; green line for THF ruined films.

62 °C. This result just agreed with the data of the thermal analysis taken by DSC and POM (**Figure 2-6**). Thus, the SRG inscription was readily erased by heating above T_i of p5Az10Me-PE4.5-Ci. This knowledge also coincides with our previous results. In 2001, in case of polymer 6Az10-PE4.5, published on advanced materials, it was said "the diffraction efficiency of the film reduced drastically around 80°C, which is in exact accord with the isotropization temperature of this liquid crystalline polymer." So do the following papers regarding to this series of azobenzene polymers. So, if without any further fixation, SRG pattern can only be maintained under T_i .

2.3.4 Photo-fixation

As shown in **Figure 2-12** (a), the device was set as same as the device used in pre-orientation of polymer films, except for the filters. In this process, 2 filters were used, one is D33S, another is a glass filter. Together they can screen out the light ranging 300-400nm wavelength (**Figure 2-12** (b)).

A SRG inscribed film was irradiated with UV light at wavelengths ranging 300 – 400nm changing the time from 1 to 40 min at room temperature (**Figure 2-13**). As indicated, during the irradiation, the absorption band of the cinnamoyl group at 280-300 nm was gradually reduced, this should be due to the proceeding of [2+2] cycloaddition reaction leading to the formation of a cyclobutane ring, known as [2+2] photo-dimerization.

The microstructures of SRGs under different irradiation energy for the crosslinking were further evaluated by AFM. By comparing them, it was found that for the photo-crosslinking, the best irradiation intensity and time were found to be 50 mW cm⁻² of 313 nm light for 15 min, respectively. **Figure 2-14** showed the UV absorption change of 4 films being crosslinked for 15, 17, 19, 20min, from which, no

significant change was noticed. Hence, crosslinking for more than 15min is considered to be meaningless.

2.3.5 Optical properties of SRG after photo-crosslinking

The grating pattern picture taken after photo-crosslinking at above conditions showed almost no change at any scale. The grating depth was also unchanged to give 130 nm, which remained the same level as observed before the photo-crosslinking. This irradiation also leads to the trans-to-cis isomerization of Az unit, however, this did not influenced the SRG structure as far as the irradiation was achieved at room temperature, namely below T_g .

2.3.6 Insolubility improvement

The course of crosslinking was confirmed by dissolving behavior in THF, a good dissolving solvent for the original p5Az10Me-PE4.5-Ci. **Figure 2-15** showed the absorption spectra obtained after rinsing in THF for films exposed to UV light at various periods. These data indicate that the UV exposure for 15 min leads to the sufficient insolubility for THF. Essentially the same results were obtained when chloroform was employed for the rinsing solvent. In theory, it is believed that this highly improved insolubility is a result of the gelling of polymer. Crosslinking of cinnamate side chain has greatly enlarged both the polymer volume and molecular weight, which turned the polymer into gel rapidly. This will also be referred to in the following paragraph.

2.3.7 Thermal stability of the SRG after crosslinking

Figure 2-16 displayed the AFM image of the photo-crosslinked SRG

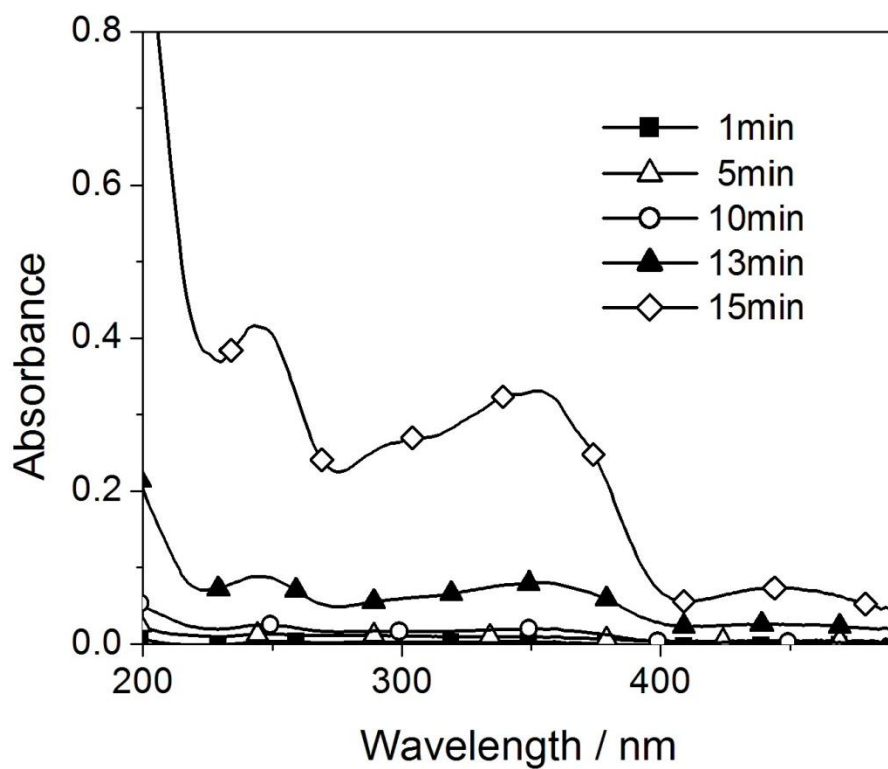


Figure 2-15 UV-vis absorption spectra of five series of films subjected to the photo-crosslinking for 1, 5, 10, 13 and 15 min and subsequently rinsed in THF.

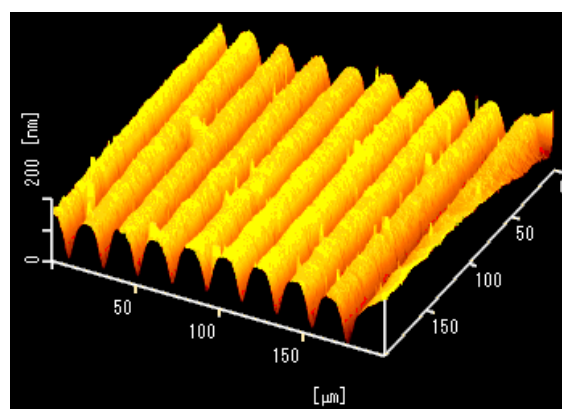
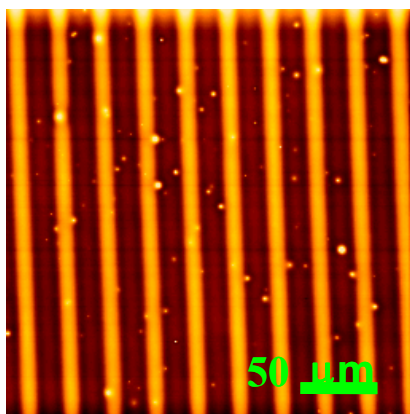


Figure 2-16 AFM image of a photo-crosslinked SRG film after immersing in THF and chloroform, and subsequent heating at 300°C for 5 min.

structure after the treatment in THF and chloroform, and subsequently heated at 300 °C for 30 min. This SRG pattern showed no significant change comparing with that of the ax-prepared SRG film as shown in **Figure 2-9**. In sharp contrast, the SRG inscribed film without photo-crosslinking could retain its pattern only up to 55 °C which is just below the T_i . After photo-crosslinking, on the other hand, the SRG pattern is able to be maintained at 300 °C without any reduction in its grating depth. In the above manners, the stability to high temperature was substantially improved, as well as the resistance to solvent exposures.

2.4 Conclusion

A photo-crosslinkable ternary Az copolymer was newly developed, in which a cinnamoyl group was introduced in the liquid crystalline Az side chain polymer. The polymer showed a favorable property of liquid crystalline nature to exert the mass transport. After pre-irradiation of 365 nm UV light followed by patterned visible light at 436 nm at 50 °C, the SRG structure was readily formed with a grating depth of 130 nm, which corresponds to nearly twice level of the initial thickness. This SRG pattern was able to be erased when heated above the isotropization temperature. Without crosslinking, the film was readily dissolved in chloroform or THF. After subsequent photo-crosslinking at room temperature, the SRG patterns remained essentially unchanged after rinsing the above solvents. The thermal stability was improved drastically, i. e., the SRG structure was not influenced after heating up to 300 °C for 30 min. it is expected that this new type of photo-crosslinkable polymer will provide wider opportunities for the application of the SRG structures.

Reference

1. K. Subramanian, V. Krishnasamy, S. Nanjundan, *Eur. Polym. J.* 2000, **36**, 2343
2. D. Feng, M. Tsushima, T. Matsumoto, T. Kurosaki, *J. Polym. Sci. A: Polym. Chem.* 1998, **36**, 685
3. D. W. Grijpma, Q. P. Hou, *J. Biomaterials.* 2005, **26**, 2795
4. S. P. Cullen, S. K. Ha, M. G. Lagally, P. Gopalan, *J. Polym. Sci. Part A: Polym. Chem.* 2008, **46**, 5826
5. A. Barichard, Y. Israeli, A. Rivaton, *J. Polym. Sci. Part A: Polym. Chem.* 2008, **46**, 636
6. D.Y. Kim, S.K. Tripathy, L. Li, J. Kumar, *Appl. Phys., Lett.*, 1995, **66**, 1166.
7. N. C. R. Holme, P. S. Ramanujam, and S. Hvilsted, *Opt. Lett.*, 1996, **21**, 902.
8. A. Natansohn, P. Rochon, *Chem. Rev.*, 2002, **102**, 4139.
9. N. K. Viswanathan, *J. Mater, Chem.*, 1999, **9**, 1941.
10. K. J. Yager, C. J. Barrett, *Curr. Opin. Solid State Mater. Sci.*, 2001, **5**, 487.
11. T. Seki, *Curr. Opin. Solid State Mater. Sci.*, 2007, **10**, 241.
12. E. Ishow, B. Lebon, Y. He, X. Wang, L. Bouteiller, L. Galmeche, K. Nakatani, K. *Chem. Mater.*, 2006, **18**, 1261.
13. O. Kulikovska, L. M. Goldenberg, J. Stumpe, *Chem. Mater.*, 2007, **19**, 3343.
14. T. Ubukata, K. Takahashi, Y. Yokoyama, *J. Phys. Org. Chem.*, 2007, **20**, 981.
15. H. Nakano, T. Takahashi, T. Kadota, Y. Shirota, *Adv. Mater.*, 2002, **14**, 1157.
16. T. Ubukata, T. Seki, K. Ichimura, *Adv. Mater.*, 2000, **12**, 1675.
17. T. Ubukata, T. Higuchi, N. Zettsu, T. Seki, M. Hara, *Colloids & Surf. A*, 2005, 257-258, **123**.
18. T. Ubukata, M. Hara, K. Ichimura, T. Seki, *Adv. Mater.*, 2004, **16**, 220.
19. N. Zettsu, T. Ubukata, T. Seki, K. Ichimura, *Adv. Mater.*, 2001, **13**, 1693.
20. N. Zettsu, T. Fukuda, H. Matsuda, T. Seki, *Appl. Phys. Lett.*, 2003, **83**, 4960.
21. N. Zettsu, T. Seki, *Macromolecules*, 2004, **37**, 8692.
22. N. Zettsu, T. Ogasawara, R. Arakawa, S. Nagano, T. Ubukata, T. Seki, *Macromolecules*, 2007, **40**, 4607.
23. T. Kimura, J-Y. Kim, T. Fukuda, H. Matsuda, *Macromol. Chem. Phys.*, 2002, **203**, 2344.
24. K. Ichimura, Y. Akita, H. Akiyama, K. Kudo, Y. Hayashi. *Macromolecules*, 1997, **30**, 901.
25. P. G. Egerton, E. Pitts, A. Reiser, *Macromolecules*, 1981, **14**, 95.
26. R. M. Kumar, R. Balamurugan, P. Kannan, *Polym. Int.*, 2007, **56**, 1230.

Chapter 3

Photoinduced Dewetting in Thin Films of Liquid Crystalline

Dendritic Azobenzene Derivatives

3.1 Introduction

Spontaneous formation of micro and nano-patterns at the surface of soft matter induced by surface instability is a unique approach in the bottom-up fabrications. In the last three decades, dewetting of thin organic films from hard substrates has received significant attentions since polymers films are extensively applied to industrial applications. Pattern generation by dewetting provides low-cost solution processing techniques to pattern and orient organic crystals, which can be an important component for organic electronic devices ^[1].

Generally, dewetting describes the rupture of a thin liquid film on a substrate (either a liquid itself, or a solid) and the formation of droplets. Theoretically, due to long range forces in particular van der Waals forces for organic liquids, a flat thin liquid film is thermo dynamically unstable when its thickness becomes small. The films can dewet via heterogeneous nucleation and growth of dry patches, forming small clusters. They can also undergo spinodal dewetting, where thermal fluctuations of a critical capillary wavelength grow exponentially and determine the characteristic feature size ^[2-4]. The factor determining the spontaneous spreading and dewetting for a drop of oil placed on a liquid substrate (water here) with ambient gas, is the so-called spreading coefficient (S). When $S > 0$, the spontaneous spreading occurs,

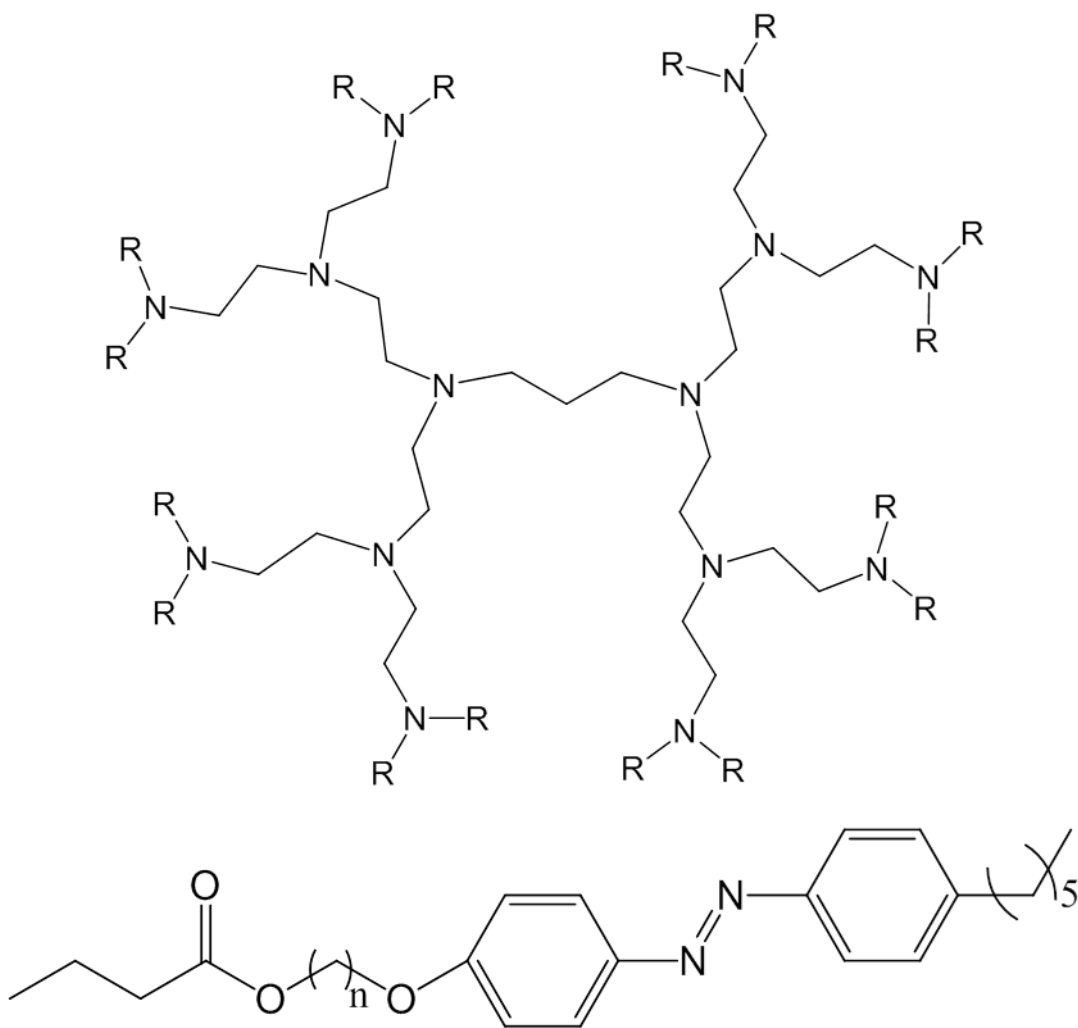


Figure 3-1 Chemical structure of amine-type dendrimers containing 16 azobenzene units in the periphery. D_n (n=6, 8, 10 and 12)

and if $S < 0$, dewetting occurs.

In most cases, annealing is adopted to proceed dewetting for a spincoated film. Annealing a metastable film increases the mobility of the polymer chain molecules and dewetting takes place. However, little examples are known for photochemically induced dewetting that occurs isothermally. Cristofolini et al. [5] reported a UV light-induced dewetting for Langmuir-Blodgett (LB) films consisting of a liquid crystalline (LC) azobenzene-containing polyacrylate. UV irradiation induces the rod-like trans to the bent cis configuration, which reduces the molecular packing stability and thus softens the material. This situation increases the film instability on the surface. They found that the dewetting process (migrating distance) is strongly dependent on the film thickness that can be precisely controlled by the LB method.

This chapter will be a report on the photoinduced dewetting phenomenon observed for LC dendritic molecules shown in **Figure 3-1**. The dendritic molecules possess the defined molecular mass and have no chance of chain entanglement among the molecules. Such systems eliminate the complexity and seem to be most suited for observation of the photoinduced dewetting behavior. We will focus on 1) energy dose dependency on the dewetting behavior, and 2) the influence of the chemical structure of the dendrimers, which are discussed with the thermophysical properties. Generally, dewetting describes the rupture of a thin liquid film on a substrate (either a liquid itself, or a solid) and the formation of droplets. Theoretically, due to long range forces in particular van der Waals forces for organic liquids, a flat thin liquid film is thermodynamically unstable when its thickness becomes small. The films can dewet via heterogeneous nucleation and growth of dry patches, forming small clusters. They can also undergo spinodal dewetting, where thermal fluctuations of a critical capillary wavelength grow exponentially and determine the characteristic feature size. The

factor determining the spontaneous spreading and dewetting for a drop of oil placed on a liquid substrate (water here) with ambient gas, is the so-called spreading coefficient (S). When $S > 0$, the spontaneous spreading occurs, and if $S < 0$, dewetting occurs.

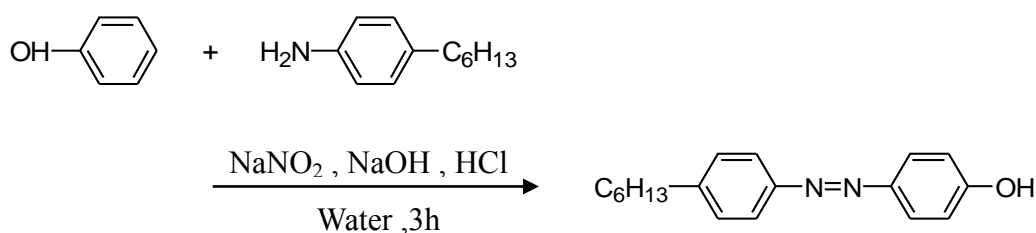
3.2 Synthesis of Dendrimers

3.2.1 Materials

Figure 3-1 shows the molecular structure of dendrimers named from D6 to D12 used in our experiment. These compounds were synthesized in Yonetake laboratory in Yamagata University. ^[9-19] The synthesis and characterizations of the dendrimer will be reported in due course. The differences between the 4 dendrimers are the length of their methylene spacer in the azobenzene unit. D6, D8, D10 and D12 have six, eight, ten and twelve methylene spacers respectively.

p-Hexylaniline (Kanto Chemicals), NaOH (Kanto Chemicals), phenol (Kanto Chemicals), NaNO₂ (Kanto Chemicals), HCl (Kanto Chemicals), 6-bromo-1-hexanol (Tokyo Kasei), KOH (Kanto Chemicals), ethanol (Kanto Chemicals), diethylether (Kanto Chemicals), triethylamine (Kanto Chemicals), acryloyl chloride (Tokyo Kasei), 2-butanon (Kanto Chemicals), chloroform (Kanto Chemicals), and poly(propylenimine)dendrimer($G = 2$) (Aldrich) were purchased and used as receive. Tetrahydrofuran (THF) was distilled from sodium-benzophenone ketyl just before use.

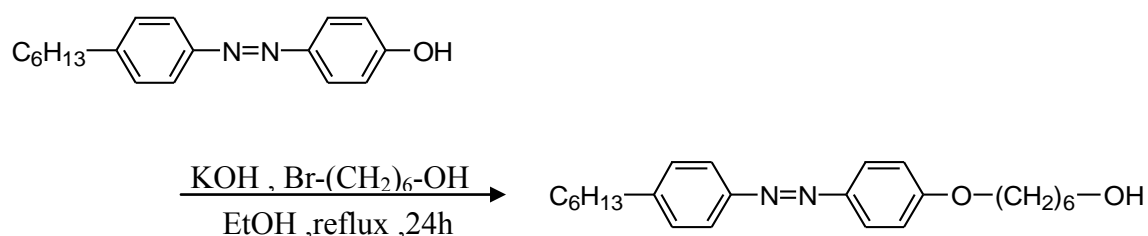
3.2.2 Synthesis of 4-(4'-Hexylphenylazo)phenol



Scheme 1

To a solution of p-hexylaniline (7.3 ml, 37 mmol) and concentrated hydrochloric acid (20ml), aqueous solution (25 ml) and NaNO₂ (4.2 g, 62 mmol) was added to the resulting blue solution. Aqueous solution (25 ml) and NaOH (3.0 g, 21mmol) and phenol (8.2 g, 37mmol) was added. Concentrated hydrogen chloride was then added dropwise until the solution became acidic. After stirring for 3h at 10°C, the precipitate was filtered, washed with water and dissolved in diethyl ether (100 ml). The ethereal solution was washed with water, dried over MgSO₄, and concentrated under reduced pressure. The residue was recrystallized from n-hexane to give brown powder. Yield 4.6g (16.4 mol, 44.2 %). ¹H-NMR (CDCl₃, 270MHz): δ (ppm) = 6.63-7.88 (s, 8H, ArH), 5.0 (1H, OH), 2.55 (t, 2H, PhCH₂), 1.29-1.62 (m, 8H, CH₂), 0.96 (t, 3H, AlkylCH₃). IR (KBr) : ν(cm⁻¹) = 1465 (Ph), 1589 (Ph), 2854 (CH₂), 2954 (CH₂), 3409 (OH)

3.2.3 Synthesis of 6-[4-(4-Hexyl-phenylazo)-phenoxy]-hexanol



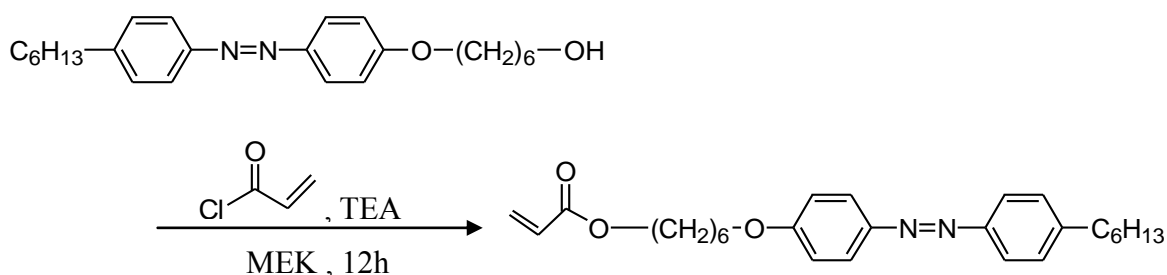
Scheme 2

A solution of 1 (5.5 g, 20 mmol), 6-bromo-1 hexanol (3.1 ml, 20 mmol), and KOH (1.1g, 20 mmol) in ethanol (30 ml) was stirred under reflux for 12h under

nitrogen. The solvent was evaporated, and the residue extracted with ether. The organic layer was washed with water, dried over MgSO₄ and concentrated. The resulting solid was recrystallized from n-hexane to give glossy yellow crystal. Yield 4.32g (11 mmol, 57.9 %) ¹H-NMR (CDCl₃, 270MHz):δ (ppm) = 0.96 (t, 3H, AlkylCH₃), 1.29- 1.71 (m, 16H, CH₂), 2.55 (t, 2H, PhCH₂), 3.65 (2H, CH₂OH), 4.0 (2H, OCH₂), 6.97-7.88 (s, 8H, ArH). IR (KBr): ν (cm⁻¹) = 1249 (Ph-O-), 1465 (Ph), 1604 (Ph), 2854 (CH₂), 2931 (CH₂), 3262 (OH), 3332 (OH)

3.2.4 Synthesis of Acrylic acid

6-[4-(4-hexyl-phenylazo)-phenoxy]-hexyl ester



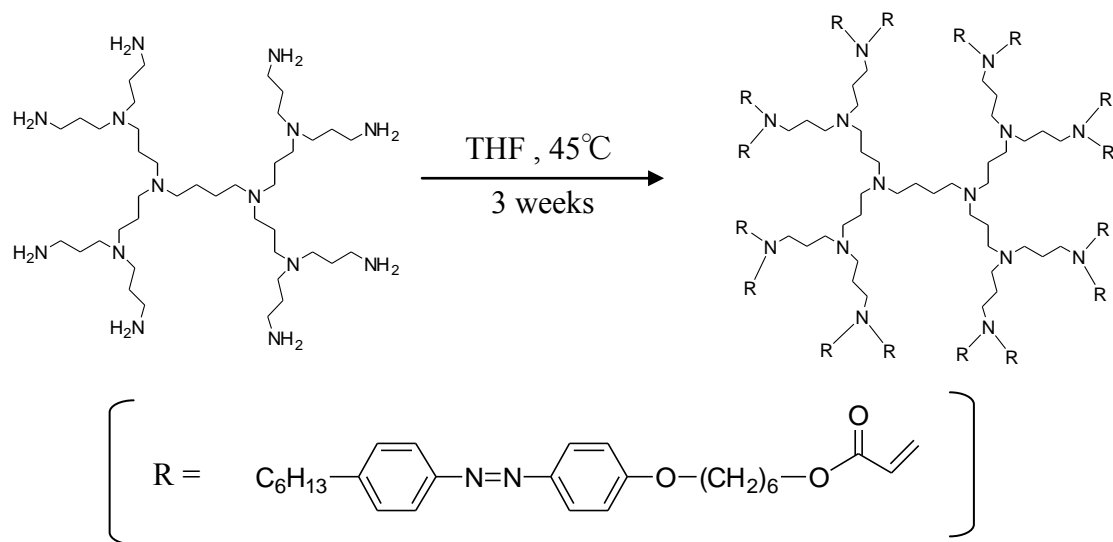
Scheme 3

To a solution of 2 (5.4g, 14 mmol) and triethylamine in 2-butanon, a solution of acryloyl chloride (1.2 ml, 14 mmol) in 2-butanon (20 ml) was added dropwise at 0°C. After stirring for 1 h at room temperature, the reaction mixture was concentrated and extracted with ether. The organic layer was washed with water, dried over MgSO₄ and concentrated under reduced pressure. The residue was recrystallized from n-hexane to give yellow powder. Yield 4.0 g (9.2 mol, 65 %). ¹H-NMR(CDCl₃, 270MHz):δ (ppm) = 0.96 (t, 3H, Alkyl CH₃), 1.29-1.71 (m, 16H, CH₂), 2.55 (t, 2H, PhCH₂), 4.15 (t, 2H, COOCH₂), 3.94 (t, 2H, PhOCH₂), 5.83 (dd, 1H, =CH), 6.13(dd, 1H, =-CH₂=CH-), 6.41 (dd, 1H, =CH), 6.67-7.88 (s, 8H, ArH). IR (KBr): ν(cm⁻¹) = 840 (C=C), 1010 (C-O-C) 1211 (Ph-O-), 1465 (Ph), 1604 (Ph), 1720 (C=O), 2861

(CH₂), 2931 (CH₂)

Anal. Calcd for C₂₇H₃₆N₂O₃ : C 74.28%, H 8.31%, N 6.42%, Found : C 74.48%, H 8.62%, N 6.35%

3.2.5 Preparation of liquid crystalline dendrimer



Scheme 4

A solution of poly(propyleneimine)dendrimer generation 2 (0.039 g, 0.51 mmol) in THF (5 ml), a solution of 3 (4.9 g, 11.2 mmol) in THF (5.0 ml) was added. The resulting solution was stirred at 45°C for 2 week under nitrogen and then poured into 500 ml of n-hexane. The precipitate was collected by filtration, and the obtained powder was purified by reprecipitation with THF / n-hexane.

Yield 3.90 g (0.50 mol, 98.8%) ¹H-NMR (CDCl₃, 270MHz): δ (ppm) = 0.96 (t, 48H, Alkyl CH₃), 1.29-1.71 (m, 304H, CH₂), 2.35 (t, 32H, CH₂C=O), 2.36 (t, 52H, CH₂-N), 2.55 (t, 32H, CH₂Ph), 2.75 (m, 32H, CH₂CH₂C=O), 3.94 (t, 32H, PhCH₂O), 4.08 (t, 32H, COOCH₂), 6.97-7.88 (s, 128H, ArH). IR (KBr): ν(cm⁻¹) = 840 (C=C), 1010 (C-O-C) 1249 (Ph-O-), 1465 (Ph), 1604 (Ph), 1735 (C=O), 2854 (CH₂), 2931 (CH₂)

Anal, Calcd for C₄₇₂H₆₇₂N₄₆O₄₈ : C 73.07%, H 8.73, N 8.30%, Found : C 71.54%, H 9.50%, N 8.47%

3.3 Methods

3.3.1 Thermal analysis.

Differential scanning calorimeter (DSC) was carried out on a DSC Q20 MO-DSC-UV under helium purging gas (0.11 MPa) at a heating/cooling rate of 2 °C min⁻¹.

3.3.2 Film fabrication.

Quartz substrates were first immersed in KOH-methanol mixture for several days for hydrophilic treatment, then washed by tap water and finally cleaned by ultrasonic treatments for 15 min while immersing in deionized water. Films were formed on the quartz substrates from chloroform solutions of D6 to D12 by spin-coating method. The spin speed was 3000 rpm. The whole process was carried out at room temperature. The initial thickness was ca. 95 nm for all samples. All films were prepared on a hydrophilic substrate.

3.3.3 Microscope observation.

The morphology of all films was observed by an atomic force microscope (Nanopics 2100, Seiko instruments) using the damping mode. Original film thickness was also obtained using the same AFM instrument by creating and measuring a scratch on the film.

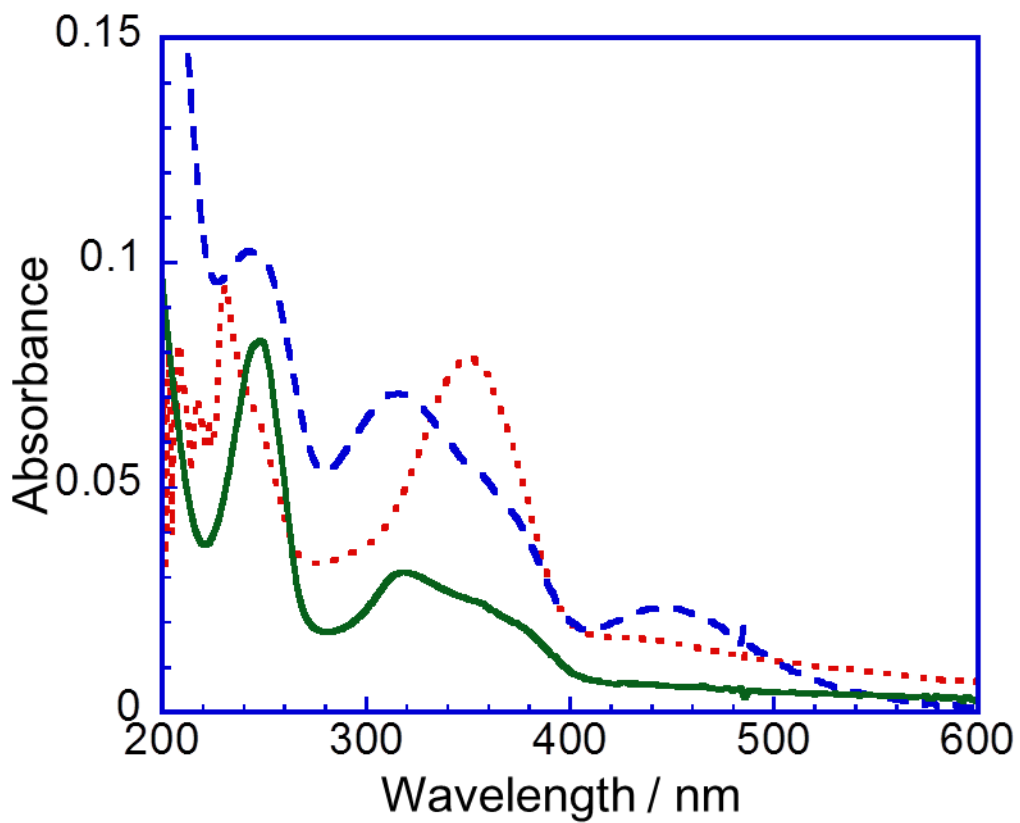


Figure 3-2 UV-visible absorption spectra of D6 in chloroform (dotted line), in a spincoast film before (solid line) and after (dashed line) UV exposure.

3.3.4 Light irradiation.

The films were later irradiated to a Xe-Hg UV lamp, Sanei-200s (non-polarized) made by San-ei Electric through a 365 nm photo filter at room temperature. Incident light intensity was adjusted to 5 mw/cm^2 , measured by a power meter. For D6 films, they were exposed to UV for 35s, 45s, 50s, 60s, 80s and 100s, while D8, D10 and D12 film were equally exposed to UV for 50s.

3.3.5 Spectroscopic measurements.

UV-vis absorption spectra were taken on an Agilent 8453 spectrophotometer (Agilent Technology). All at room temperature, using blank substrate as reference, sample films UV-vis absorption were measured.

3.4 Results and conclusions

3.4.1 UV-vis. absorption spectroscopy

Figure 3-2 shows the UV-visible absorption spectra of D6 in chloroform (dash-dotted line), of a spincast film before (solid line) and after (dash line) UV exposure. The absorption peak of the $\pi\text{-}\pi^*$ long-axis transition of azobenzene in chloroform was positioned at 360 nm, while that of the spincast film was located at 320 nm. This fact indicates that the azobenzene unites form H-type aggregation partially in case of the spincast thin film state. The molecular orientation of the azobenzene units of the spincast film can be roughly estimated by the ratio of absorption intensities of the $\pi\text{-}\pi^*$ long-axis transition of azobenzene (around 340 nm) to the $\pi\text{-}\pi^*$ transition of phenyl (244 nm, often expressed as $\phi\text{-}\phi^*$) bands, since the direction of the $\pi\text{-}\pi^*$ long-axis transition of azobenzene is directly dependent while

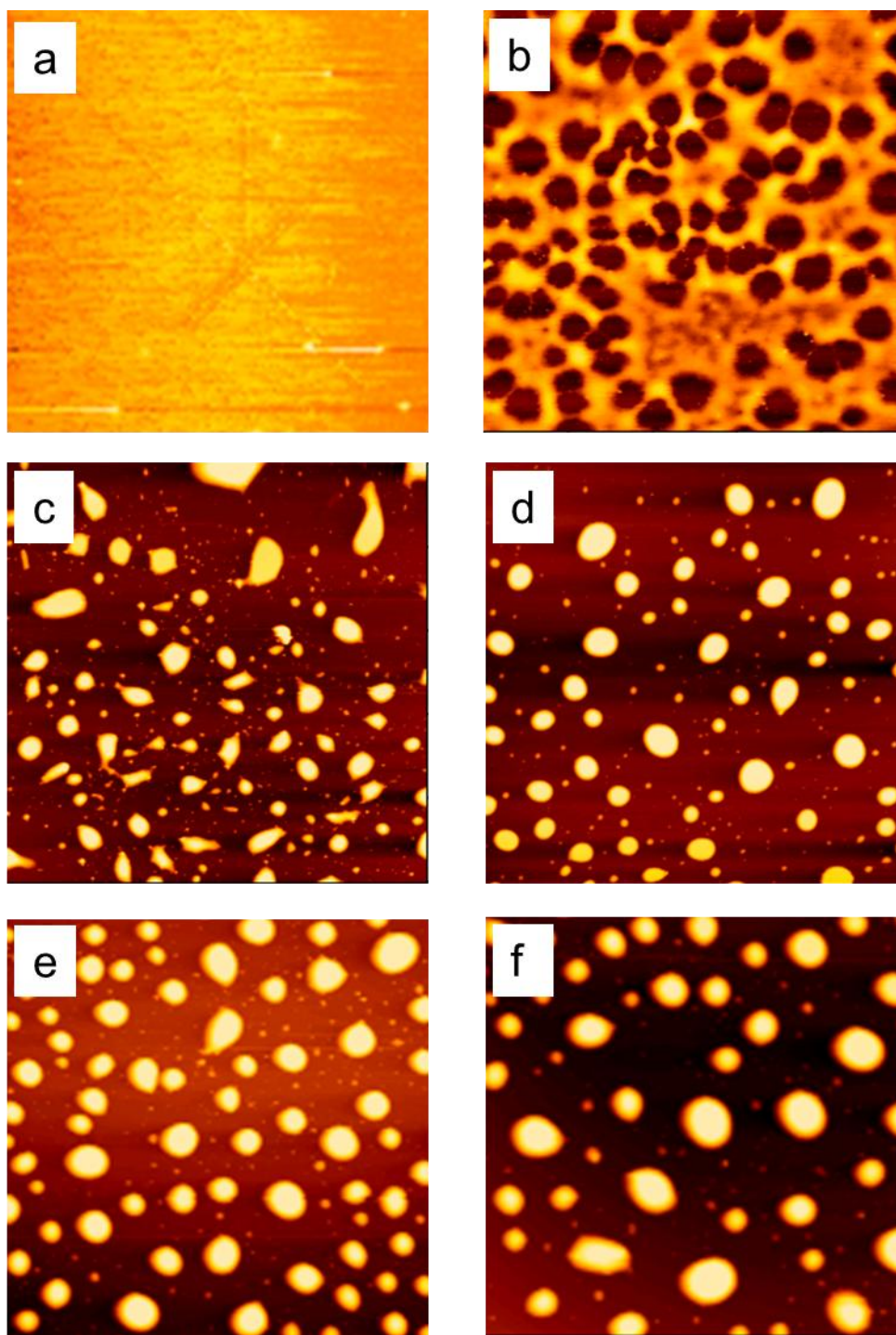


Figure 3-3 Dewetting morphologies ($100\ \mu\text{m} \times 100\ \mu\text{m}$ topographical AFM images) with UV irradiation period for D6 at room temperature. The images from a to f correspond to the irradiation period of 0s (initial film), 35s, 45s, 60s, 80s and 100s, respectively, at the same UV intensity of $5\ \text{mW}/\text{cm}^2$.

that of the π - π^* transition of phenyl is essentially insensitive to the azobenzene orientation. The ratios of $A_{\pi-\pi^*}$ (azobenzene)/ $A_{\pi-\pi^*}$ (phenyl) in chloroform solution and for the spin-cast film were 0.9 and 0.6. These spectral data indicates that the hydrophobic trans-azobenzene units have arranged mostly perpendicular to their substrates of the formed spin-cast films. For the film after UV exposure, the n - π^* of the cis-azobenzene absorption peak appeared at 450 nm. Obviously, the trans to cis photo-isomerization underwent in the spin-cast film by the irradiation of UV light. [6, 7] The grazing angle incidence X-ray measurements for a D12 film have revealed that the spin-cast film adopts the layer structure with a layer spacing of 3.7 nm [8], indicating that the layer consists of a bilayered smectic structure of perpendicularly oriented azobenzene units with respect to the substrate plane. It is reasonable to postulate that the same molecular packing is attained in the thin film of D6.

3.4.2 Photoinduced dewetting behavior in D6

Unlike the rod-like trans-azobenzene, the molecular packing of the cis-azobenzene units are less ordered, which is known to soften the film after UV irradiation. The dewetting was typically observed for D6. At room temperature, UV-irradiated azobenzene films turned to be a less stable liquid state. This effect is similar to what is frequently observed by annealing.

Figure 3-3 shows the topographical AFM images (100 nm x 100 nm) in the photoinduced dewetting process of D6 films. In **Figure 3-4**, the average height of the formed bumps is plotted against the increase of the energy dose. Interestingly, the height of the bumps formed by the dewetting were almost uniform regardless of the domain size.

This situation rationalizes the profile in **Figure 3-4** to be a reliable and

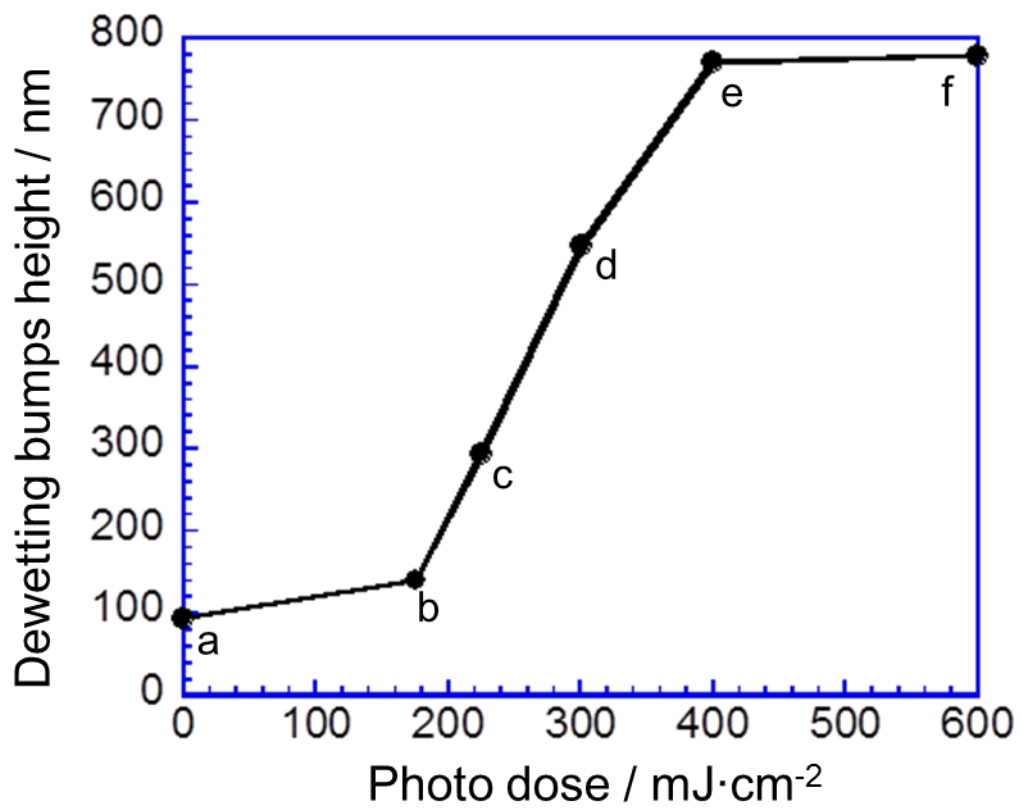


Figure 3-4 Height of the dewetting bumps vs. UV photon dose on a D6 film which has an initial thickness of 95 nm (a). Plots from a to f are obtained from the AFM data shown in Figure 3-3.

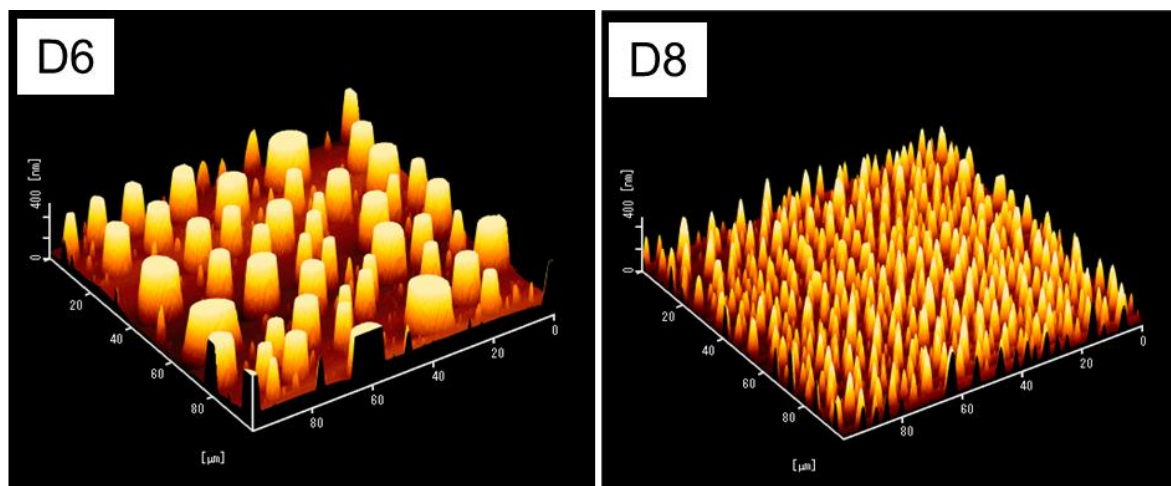


Figure 3-5 AFM images (100 μm x 100 μm area) of the bumps after dewetting for the D6 and D8 films at room temperature. Photon dose for both films are 250 mJ/cm^2

meaningful. Initially, the film was flat with 95 nm thickness (a). The influence of UV photon dose on the dewetting behavior was examined for films in the same conditions. UV exposure energy was controlled by changing the duration of UV exposure with a fixed intensity of 5 mW/cm². The dewetting bumps appeared clearly and spontaneously after UV exposure of 175 mJ/cm² (b, 5mW/cm² for 35 s irradiation). At 225 mJ/cm², continuous film domains no longer existed (c). With the exposed energy increased, the average morphological area of dewetting bumps shrank. Above 300 mJ/cm², the morphology was observed as round domains of diameters of some ten μm, and virtually unchanged (d). However, the area of the domains became larger and the height increased considerably. When UV dose reached 400 mJ/cm², the morphological change finally became fixed (e). To our surprise, the height finally reached 771 nm at 400 mJ/cm², which corresponds to ca. 8-fold of the initial thickness. Even by increasing the photon dose up to 600 mJ/cm², the morphology and the height of dewetting bumps remained no change (f). **Figure 3-4** indicates a sigmoidal shape, suggesting that the dewetting process proceeds in a highly cooperative manner. The mass migration proceeded only when the UV was irradiated. The migration did not occur in the dark even if the film involves the cis-isomer. These results imply that the migration takes place only when the film is activated by UV irradiation.

3.4.3 Dependence of dendrimer structure

The dewetting behavior was found to be strongly depending on the dendrimer structure. Both D6 and D8 showed dewetting behaviors at room temperature as shown in **Figure 3-5**. But nothing happened morphologically for D10 and D12 when exposed to UV (data not shown). This discrepancy can be related to their thermophysical properties.

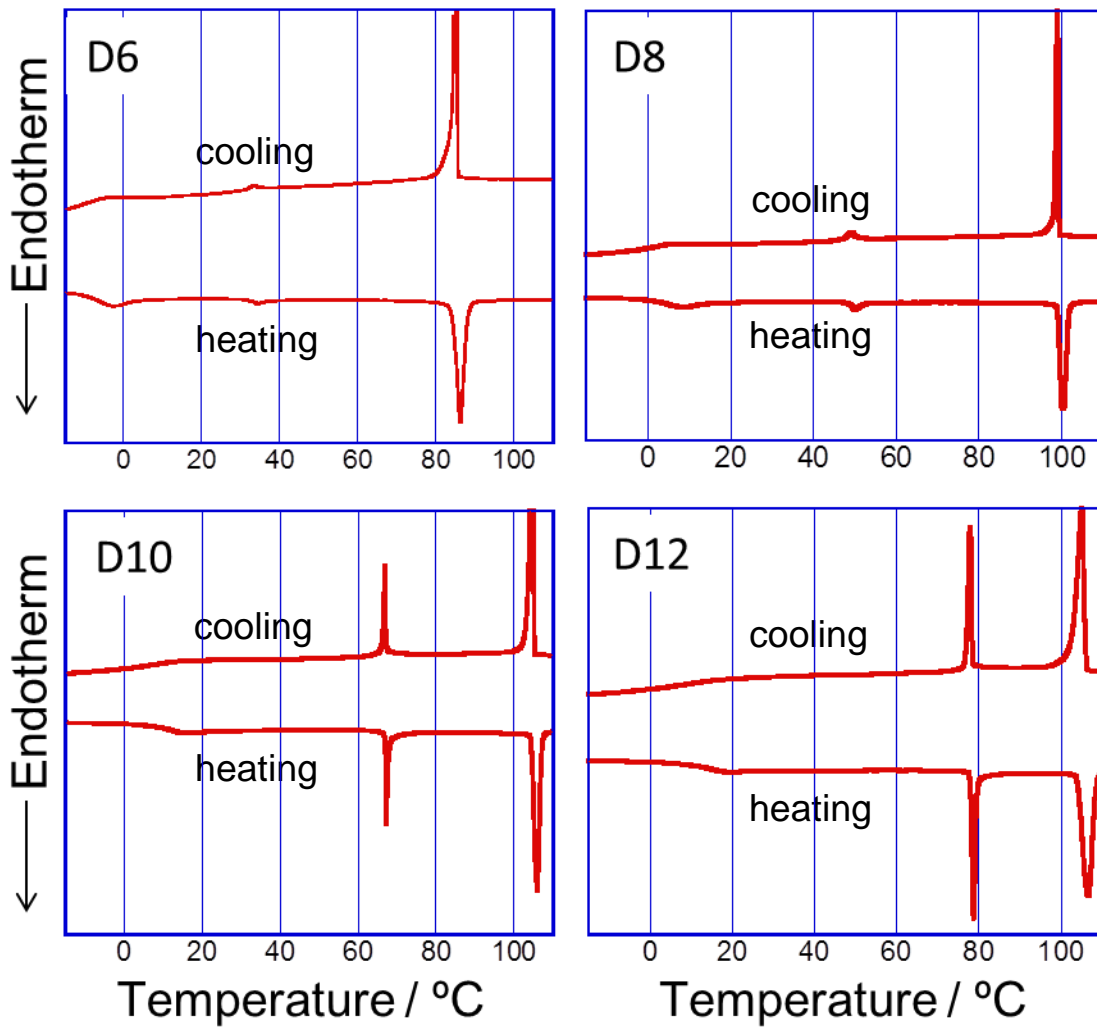


Figure 3-6 DSC curves of D6, D8, D10 and D12.

The DSC profiles from D6 to D12 in the trans-azobenzene form are displayed in **Figure 3-6**. With increasing methylene spacers, the glass transition temperature (T_g), the transition temperature from SmB to SmA, and that from SmA to isotropic phase became higher accordingly. In the heating process, D6, D8, D10, D12 showed the T_g at $-8\text{ }^\circ\text{C}$, $8\text{ }^\circ\text{C}$, $14\text{ }^\circ\text{C}$ and $17\text{ }^\circ\text{C}$, respectively. The phase transition temperature from SmB to SmA enhanced as $33\text{ }^\circ\text{C}$, $48\text{ }^\circ\text{C}$, $65\text{ }^\circ\text{C}$ and $77\text{ }^\circ\text{C}$ for D6, D8, D10 and D12, respectively. In the same way, the phase transition temperature from SmA to isotropic increased from $83\text{ }^\circ\text{C}$, $100\text{ }^\circ\text{C}$, $105\text{ }^\circ\text{C}$ and $106\text{ }^\circ\text{C}$ for the same order. The dewetting is induced by an enrichment of the cis-isomers, therefore, the ‘real’ thermal properties of the material that contributes the dewetting process cannot be directly measured. However, the thermal data for the pure trans-azobenzene state can be reasonably related to the dewetting behavior. Since the UV photoirradiation is achieved at room temperature for all cases, the increasing the transition temperatures should impede the mass transfer upon dewetting. It seems that the molecular packing order of SmB (smectic LC phase possessing a hexatic order) in the trans-azobenzene strongly governs whether the dewetting proceeds or not. The enthalpy change of the SmB to SmA phase ranging $60\text{ }^\circ\text{C}$ to $70\text{ }^\circ\text{C}$ sharply became pronounced for D10 and D12. In any event, the precise understanding needs the knowledge of the thermal properties of the film involving the cis-isomers, which will be the subject of future work.

As indicated in **Figure 3-5**, the migration distance significantly differed from D6 to D8, which exhibits a large change in the bump size features after dewetting. Consequently, D8 provided much smaller domains (right), one order of magnitude smaller than those of D6. This can be also connected to the higher phase transition behavior of D8. The molecular mobility should be more suppressed in the D8 film

due to the higher molecular packing order. Cristofolini et al. [5] discussed the migration distance with the change in film thickness. In the present case, the migration distance can be clearly related with the molecular structure.

3.5 Conclusions

This work proposed a new photoinduced dewetting process observed in dendritic azobenzene derivatives. UV light-induced dewetting occurred for compounds with shorter spacer length ($n=6$ and 8) in the azobenzene unit. For longer spacer compounds ($n=10$ and 12), the more ordered molecular packing seems to suppress the photoinduced dewetting and mass migration at room temperature as suggested by DSC measurements. In the case of D6 ($n=6$), the dewetting proceeded after an induction period, and the migration and the height enhancement of the bumps occurred in the UV exposure range from $175 - 400 \text{ mJ/cm}^2$. This suggests that the mass migration occurs in a cooperative manner. The mass migration was very efficient and, to our surprise, the saturated height after dewetting reached ca. 8-fold of the initial film thickness. Such high mobility of the material migration is probably due to the absence of chain entanglement which is characteristic in dendritic polymeric materials. These materials are fascinating to apply for photoinduced mass migration upon patterned irradiation using a photomask^[6,7]. The approach in this direction is now underway and will be reported in due course.

References

- [1]. Menard, E., Meitl, M. A., Sun, Y., Park, J., Shir, D. J., Nam, Y., Jeon, S., Rogers, J. A. (2007). *Chem. Rev.*, *107*, 1117.
- [2]. L. Xue, L. & Han Y. (2011). *Prog. Polym. Sci.*, *36*, 269.
- [3]. Rosen M. J. (2004). *Surfactants and Interfacial Phenomena* (3rd ed.): Hoboken,

New Jersey.

- [4].Karapanagiotis, I., Gerberich, W. W. (2005). *Surface Science*, 594, 192.
- [5].Crustofolini, L., Fontana, M. P., Berzina, T. & Camorani P. (2003). *Mol. Cryst. Liq. Cryst.*, 398, 11.
- [6].Nishizawa, K., Nagano, S. & Seki., T. (2009). *Chem. Mater.*, 21, 2624.
- [7].Li, W., Nagano, S. & Seki, S. (2009). *New J. Chem.*, 33, 1343.
- [8].Lin, T., Nagano, S. & Seki, T., unpublished result.
- [9].D.A. Tomalia, A.M. Naylor, W.A. Goddard. *Angew. Chem., int. Ed. Engl.*, 29, 138 (1990)
- [10].K. Suzuki, O. Haba, R. Nagahata, K.Yonetake, M, Ueda. *High Perform. Polym.*, 10, 231 (1998)
- [11].K. Yonetake, K. Suzuki, T. Masuko, T. Morishita, R. Nagahata, M. Ueda. . *High Perform. Polym.*, 10, 373 (1998)
- [12].K. Yonetake, T. Masuko, T. Morishita, K. Suzuki, M. Ueda, R. Nagahata. *Macromolecules*, 32, 6578 (1999)
- [13].O. Haba, K.Okuyama, K. Yonetake. *Mol. Cryst Liq. Cryst.*, 364, 929 (2001)
- [14].O. Haba, K.Okuyama, H. Osawa, K. Yonetake. *Liq. Cryst.*, 32, (2005)
- [15].K. Tsuda, G. C. Dol, T. Gensch, J. Hofkens, L. Latterini, J. W. Weener, E. W. Meijer, and F. C. De Schryver. *J. Am. Chem. Soc.*, 122, 3445 (2000)
- [16].A. Bobrovsky, S. Ponomarenko, N. Boiko, V. Shibaev, E. Rebrov, A. Muzafarov, J. Stumpe. *Macromol. Chem. Phys.*, 203, 1539, (2002)
- [17].D. Patton, M. K. Park, S. wang, R. C. Advincula. *Langmuir*, 18, 1688, (2002)
- [18].T. Ikeda. *J. Matter. Chem.*, 13, 2037, (2003)
- [19].A. Bobrovsky, A. Pakhomov, X. –M. Zhu, N. Boiko. V. Shibaev, J. Stumpe. *J. Phys.Chem.B*, 106, 540, (2002)

Chapter 4

Hierarchical Structure Formation in SRG Process of Azobenzene Dendrimers

4.1 Introduction

Inspired by the dewetting behavior of dendritic azobenzene polymers described in Chapter 3, the SRG formation of those dendrimers has been preceded and a series of new patterns with self-assembled hierarchical structure were discovered, which has never been reported so far. **Figure 4-1** shows the AFM pictures of both the photo mask which was used and the resulted SRG pattern with a unique hierarchical structure.

It was assumed that such kind of hierarchical patterns are most possibly caused by the dewetting behavior of dendrimer films. If this assumption is right, they should share a lot in common. So spin-cast films ranging from D6 to D12 were fabricated. Using the UV-inscription method which was mentioned in Chapter 1, experiments were carried out to inscribe SRG patterns on to the films. Just as expected, only by using D6 and D8, SRG patterns with hierarchical structures could be achieved. But for D10 and D12, they performed as well as normal linear materials, resulted only normal SRG patterns. More detailed introductions of both SRG and dewetting can be found in the former Chapters. little examples are known for photochemically induced dewetting that occurs isothermally. In particular, need to be mentioned is that Cristofolini et al. ^[1] reported a UV light-induced dewetting for

Photo mask

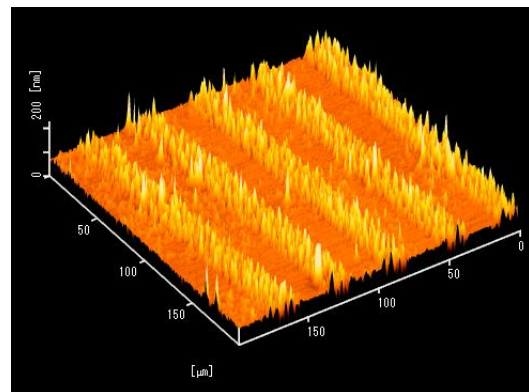
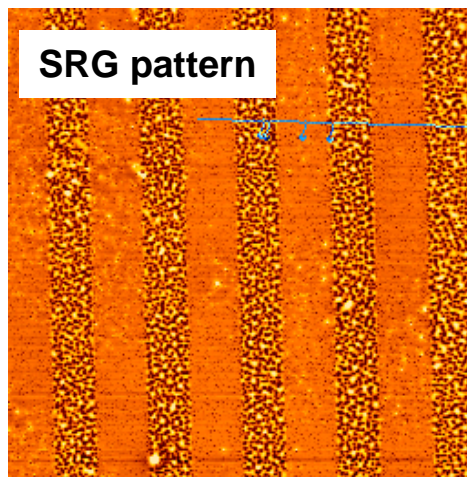
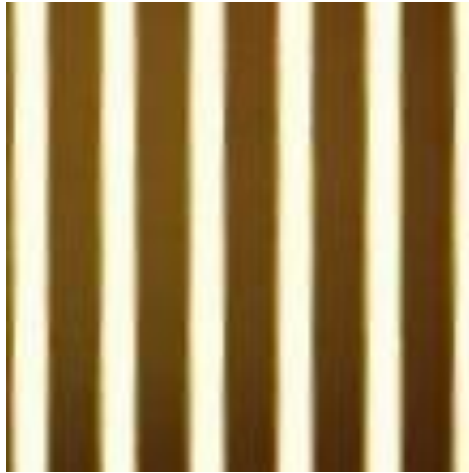


Figure 4-1 Typical hierarchical SRG pattern resulted from D6 film.

Langmuir-Blodgett (LB) films consisting of a liquid crystalline (LC) azobenzene-containing polyacrylate.

4.2 Experimental

4.2.1 Materials

The Material used for SRG formation in this chapter is D6, the dendritic material mentioned in Chapter 3.

4.2.2 Methods

Thermal analysis. Differential scanning calorimeter (DSC) was carried out on a DSC Q20 MO-DSC-UV under helium purging gas (0.11 MPa) at a heating/cooling rate of 2 °C min⁻¹. Polarized optical microscopic (POM) observations were made using a BX51 (Olympus Technology). A polarizing microscope has a pair of polars (polarizing devices) in the optical train. The first polar (polarizer) defines the initial plane of polarization for light entering the microscope and is located between the illuminator and the condenser. The other polar (analyzer) is placed between the objective and the ocular tube and defines the plane of polarization of the light reaching the ocular.

Film fabrication. D6 thin films were prepared by spin-coating method. The quartz substrates were formerly cleaned by sequential ultrasonic treatments for 15min immersing in the following fluids, THF, saturated KOH/methanol, deionized water. After dried in air, films were remained on the surface of substrate. Polymer was dissolved into THF at a ratio of 2wt%. Then, on cleaned quartz substrates (1cm×1.5cm), films were fabricated by spin-coating this solution at 2000rpm for 30s. After that, films were dried in air for 10 minutes at room temperature.

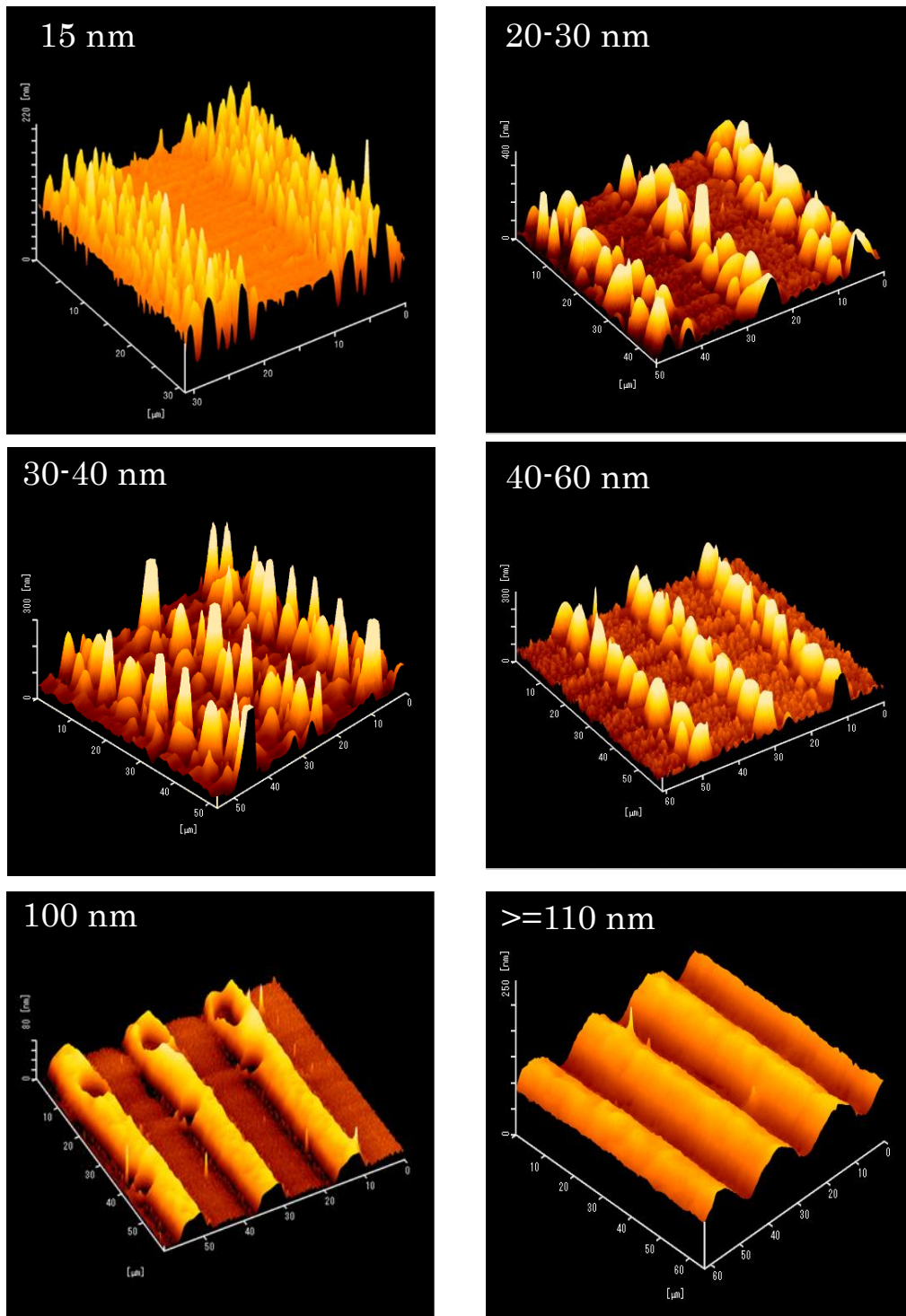


Figure 4-2 Thickness dependent SRG morphology of D6 at room temperature. with the same UV photon dose of $5\text{mW} / \text{cm}^2 \times 50\text{s}$.

Microscope observation. The morphology of all films was observed by an atomic force microscope (Nanopics 2100, Seiko instruments) using the damping mode. Original film thickness was also obtained using the same AFM instrument by creating and measuring a scratch on the film.

Light irradiation. The films were later irradiated to a Xe-Hg UV lamp, Sanei-200s (non-polarized) made by San-ei Electric through a 365 nm photo filter at room temperature. Incident light intensity was adjusted to 5 mw/cm^2 , measured by a power meter. The photo mask used for SRG formation was a stripe patterned photo mask with gaps of $10 \text{ }\mu\text{m}$.

Spectroscopic measurements. UV-vis absorption spectra were taken on an Agilent 8453 spectrophotometer (Agilent Technology). All at room temperature, using blank substrate as reference, sample films UV-vis absorption were measured.

4.3 Results and discussion

4.3.1 Thickness dependent hierarchical SRG

In particular, the experimental works were focused on the SRG inscription of D6 spin cast films. A lot of D6 films with varies of thicknesses were prepared and exposed to photo mask patterned UV at room temperature to discover the regular rule behind their morphology changes. The UV intensity is 5 mW / cm^2 , with equally 50 seconds' exposure for each one. Luckily, it was spotted that with the other conditions all the same, the initial film thickness played an important role in the morphological change of the hierarchical structures.

As shown in **Figure 4-2**, when the film is initially a thin film about 15 nm, the self-assembled dewetting domains are sharp, brush liked, with the highest density.

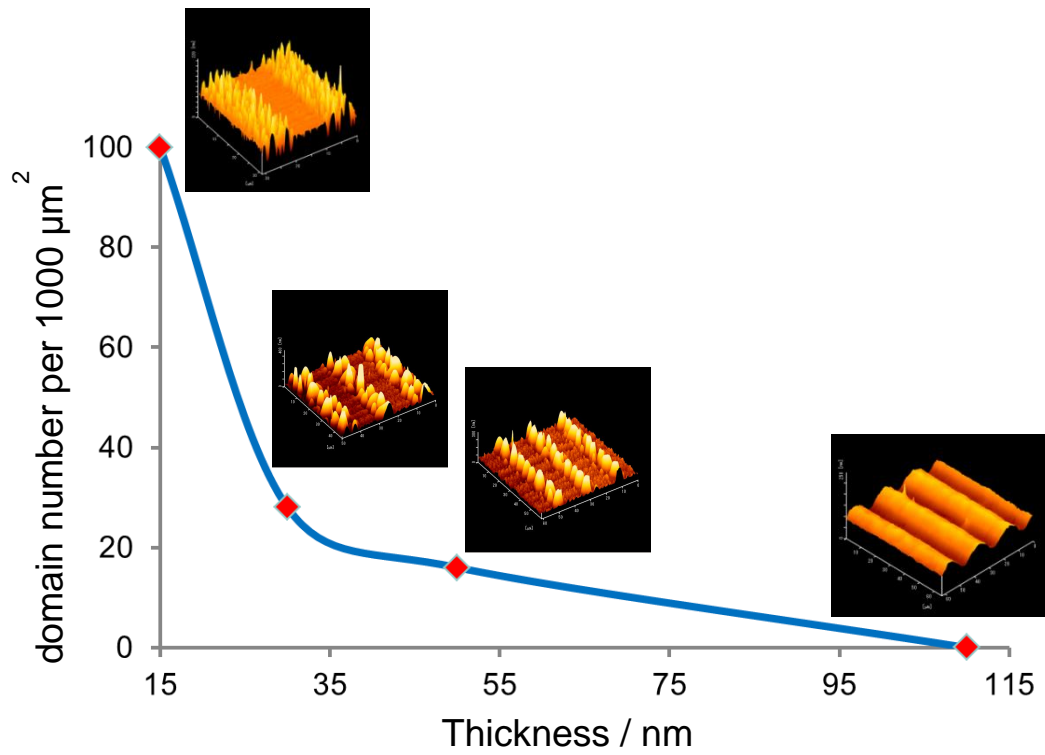


Figure 4-3 Domain numbers changed non-linearly with the increasing of film thickness.

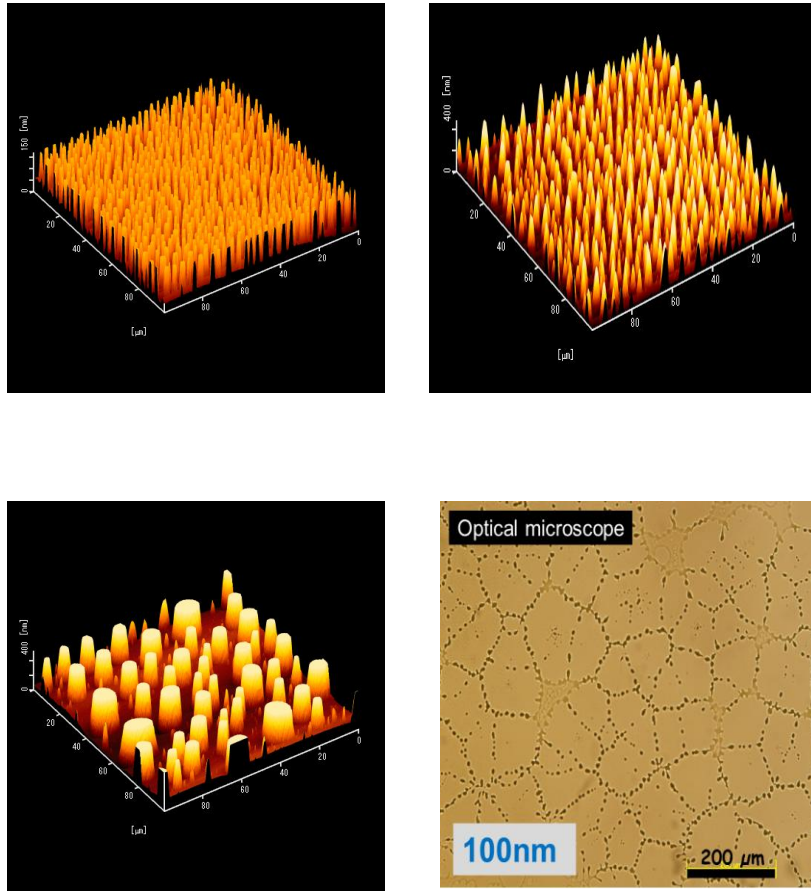


Figure 4-4 Thickness dependent dewetting morphology of D6 at room temperature. with the same UV photon dose of $5\text{mW} / \text{cm}^2 \times 50\text{s}$

The average diameter of the dewetting domains is 1-3 μm , which is also the smallest. The number of domains in every 1000 μm^2 is about 100 as counted, which is the highest. When the film thickness is increased to 20-30 nm, the hierarchical domains become a typical double-column well-arranged structure. The average domain diameter increased to 3-5 μm . The domain number remarkably decreased to 25 correspondingly in every 1000 μm^2 . Later, when the film thickness reached 40-60 nm, the hierarchical pattern showed another typical structure which has a single column dewetting domains that which was named as a crocodile pattern, since its particular shape looks exactly like the back leather of a crocodile. The average domain diameter increased to 5-8 μm . correspondingly, the domain numbers decreased again to 13. As expected, when the film thickness reached 100 nm, the hierarchical morphology disappeared significantly, SRG pattern started to be observed as common ones. Not surprisingly, the SRG pattern turned to be exactly as normal ones without any hierarchical pattern when the film thickness became 110 nm.

According to the decrease of average domain numbers in every 1000 μm^2 , a plot (**Figure 4-3**) was done to review the regular changing law. From the plot, a classic cotangent curve is approximately observed. That means, with the film thickness increased, the domain numbers decreased non-linearly.

4.3.2 Thickness dependent dewetting of D6

To confirm such kind of morphological change as a hybrid of both photoinduced SRG and photoinduced dewetting, which has never been reported, another group of pictures (**Figure 4-4**) were taken. The pictures here are to review the thickness dependence of photoinduced dewetting behavior. 4 spin-cast films with their initial thickness of 20nm, 50 nm, 90 nm and 100 nm are prepared and exposed to

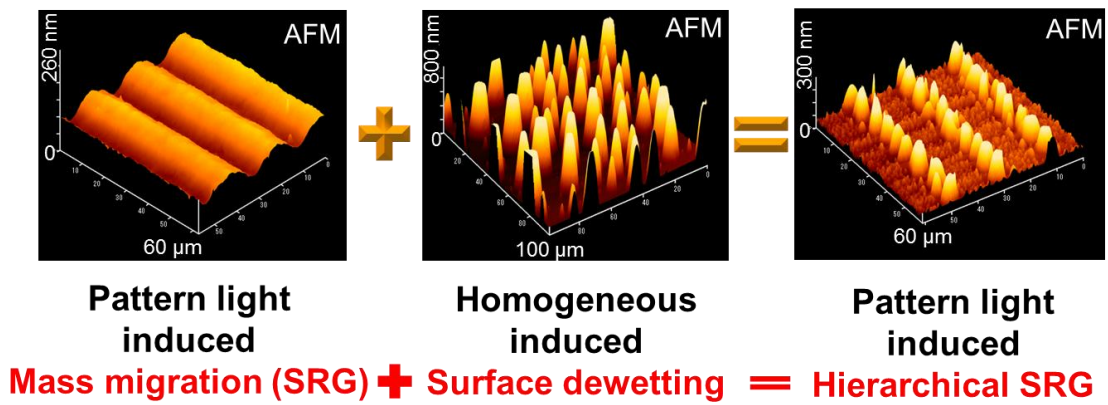


Figure 4-5 A new proposal of the formation of hierarchical SRG as a hybrid of mass migration and self dewetting.

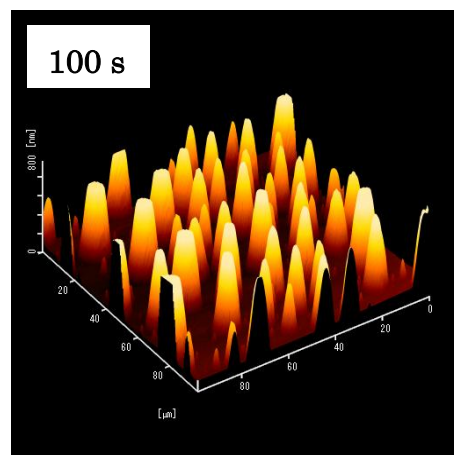
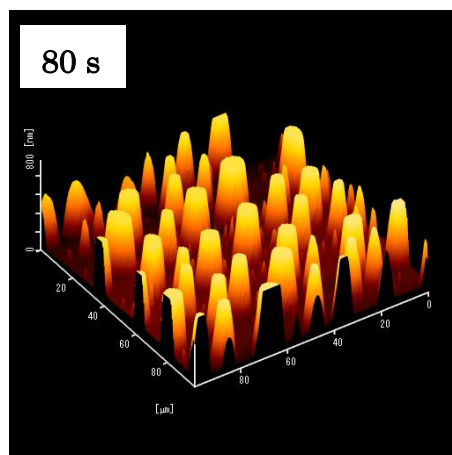
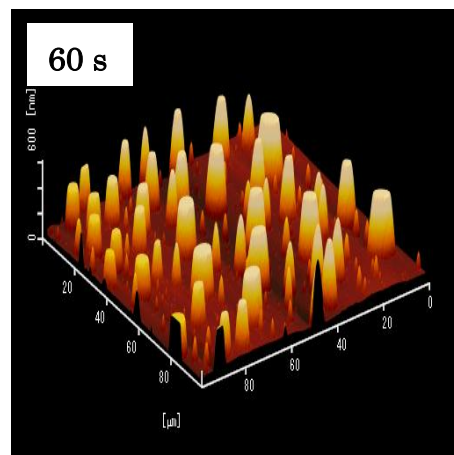
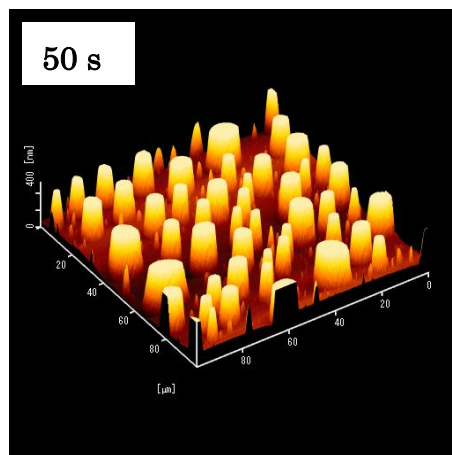
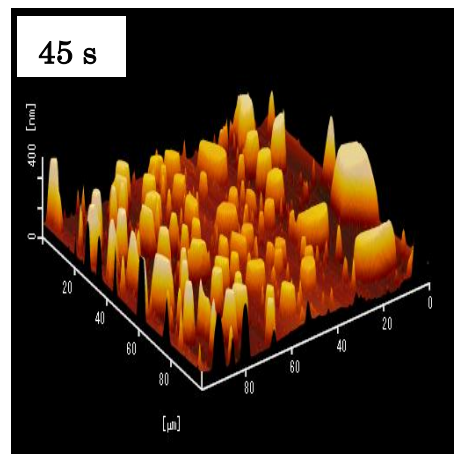
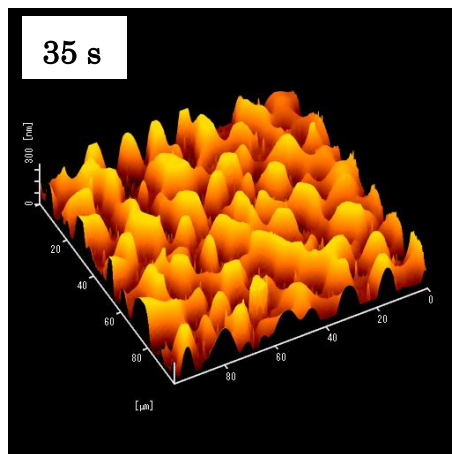


Figure 4-6 UV-exposure time related dewetting morphology of D6 at room temperature with the same UV intensity of $5 \text{ mW} / \text{cm}^2$. (Initial thickness: 90 nm)

homogenous UV (365 nm) for 50 seconds at an intensity of $5 \text{ mW} / \text{cm}^2$. From the pictures it can be seen clearly that the dewetting domain size increased significantly with the increasing of the initial film thickness, which is exactly the same with the result showed in **Figure 4-2**. So does the domain density also increased correspondingly like **Figure 4-2**. On a thin film, the dewetting domains arranged like a polymer brush, while on a thick film, the domains packed more like bumps, more individual, fatter and stronger. This phenomenon showed extremely similar to the pictures showed in **Figure 4-2**. This proved that the hierarchical structures are surely related to the photoinduced dewetting mechanism in a molecular level, as is shown in the **Figure 4-5**.

Need to be mentioned is that such kind of hybrid SRG has not been reported so far, so to study the mechanism of the process during photoinduced dewetting, another group of pictures were taken (**Figure 4-6**). Pictures displayed in **Figure 4-6** are the gradual change of morphological dewetting domains during homogenous UV exposure. With an intensity of $5 \text{ mW} / \text{cm}^2$ at room temperature, duration ranging from 35 s to 100s, 3D morphological changes were displayed. By comparing them, especially the pictures of 50 s and 100 s, the dewetting domain were growing from a flat top cylinder shape to a sharp top cone shape. Meanwhile, their bottom size remained mostly the same. In fact, this explained that how did the huge difference of their heights appeared in the last chapter (**Figure 4-4**). With the same bottom area and the same volume, a cone surely has no problem to reach 3 times height of a cylinder.

4.3.3 Mechanism assumption

Based on this idea, a new assumption of the mechanism for the growth of dewetting domains over time can be concluded, which has to explain the

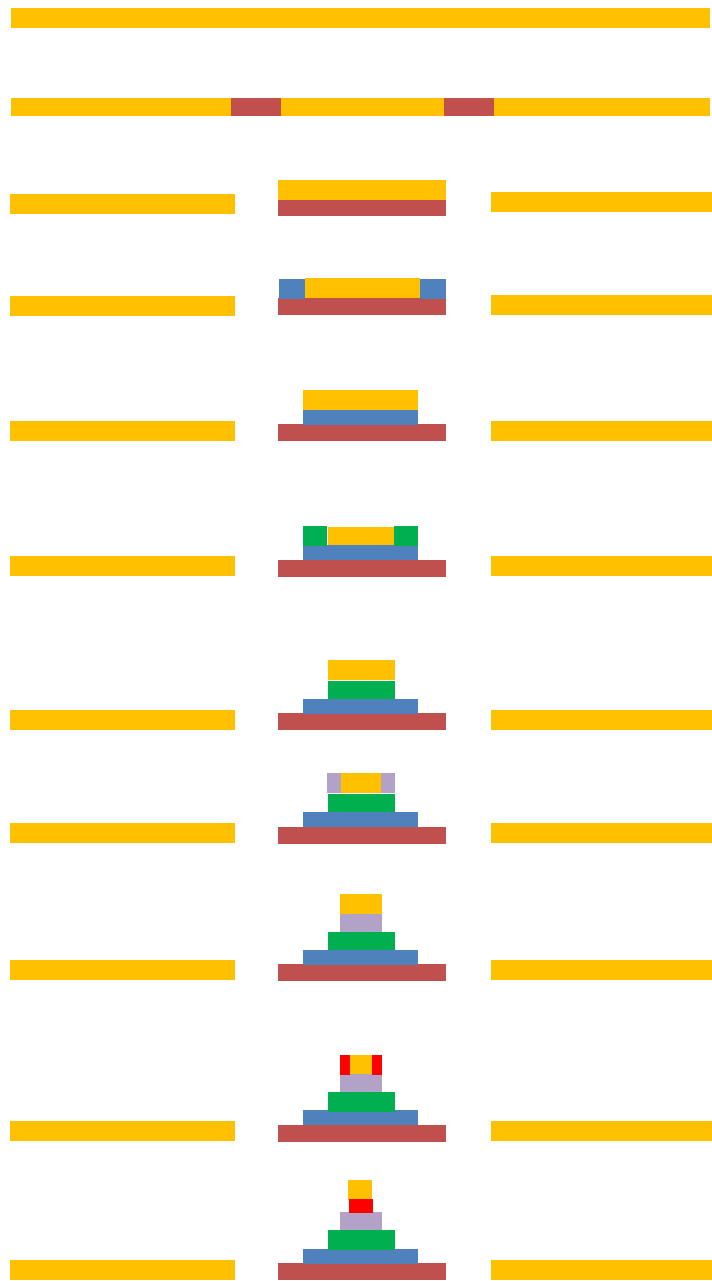


Figure 3-7 How the cylinder domain grew to a cone domain.

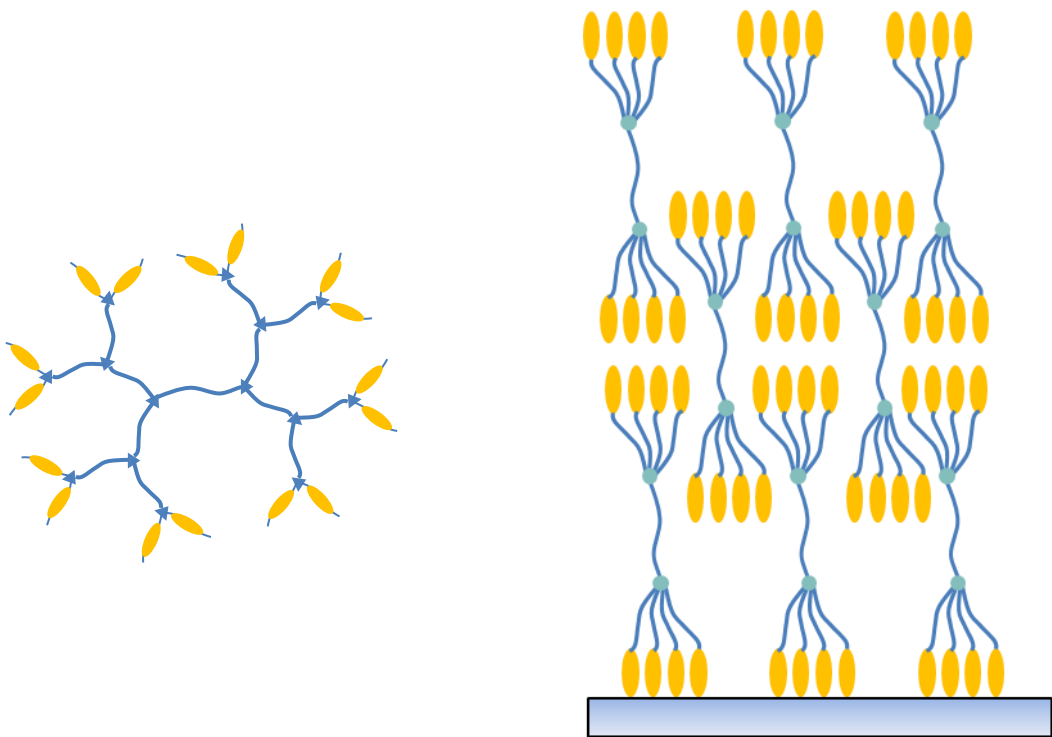


Figure 3-8 Structure model of dendrimers packing in a spin-cast film. ^[3]

extraordinary flat top shape during short period UV exposure, and the opposite sharp top during long period UV exposure as **Figure 4-7**. At the very beginning, some parts of the film started to collapse spontaneously and randomly at UV exposure. These collapsed parts moved towards their neighbor film part and hid beneath them to keep a low energy and less excited state, which actually pushed this neighbor upwards and formed a new layer, which can be called as a neighbor layer. The flat tops in 3D AFM pictures are just the top surface of that neighbor part. Later, with more UV exposure, some parts of this neighbor layer started to collapse and reproduced the scene of their original layer. By repeating such a collapse-hide-push process, more and more layers were formed beneath the initial film. Moreover, such kind of accumulating mechanism might have a relationship with their packing method, which is displayed in **Figure 4-8**.

4.4 Conclusions

This chapter proposed a newly discovered photo induced hierarchical SRG formation in spin-cast azobenzene dendrimers. At room temperature, photo mask patterned UV light induced hierarchical SRG patterns appeared in case of D6 and D8 which have shorter spacer length, but not in case of D10 and d12. This is just the same with the result which is reported in Chapter 3. Such kind of hierarchical SRG formation is caused by the high mobility involved by photoinduced dewetting, which is studied in Chapter 3. For the D6 films, the highly improved mobility lead to varies of SRG patterns which showed a strong relationship between the resulted hierarchical domains of SRG and the original film thickness. These particular SRG patterns have a macro shape following their photo mask which is driven by the patterned UV. But in micro level, varies of hierarchical dewetting domains ranging

from 1 μm to 8 μm were observed. This suggests that the unique SRG pattern were driven by both photoinduced mass migration and photoinduced dewetting behavior. It can be assumed that such kind of hybrid mechanism of SRG formation method might support a further research in the study of hierarchical SRG formation. ^[2]

References

- [1].Crustofolini, L., Fontana, M. P., Berzina, T. & Camorani P. (2003). *Mol. Cryst. Liq. Cryst.*, 398, 11.
- [2].Nishizawa, K., Nagano, S. & Seki., T. (2009). *Chem. Mater.*, 21, 2624.
- [3].Lin, T., Nagano, S. & Seki, T., unpublished result.

Chapter 5

Summary

As a conclusion, our whole work concentrated on the change of the mobility of SRG patterns. By applying photo-crosslink, the mobility was decreased and the SRG patterns were fixed. By involving photoinduced dewetting, we increased the mobility and created many unusual hierarchical SRG patterns.

Correspondingly, Chapter 1 is a general introduction on various characterizations of SRG, especially the highly sensitive SRG inscription on LC azobenzene derivatives.

Chapter 2 is the photo crosslinking method used in our experiment for the fixation of SRG patterns. A new polymer was designed and synthesized for this purpose. The SRG pattern was successfully inscribed on this material and lateral photo crosslinking fixation was also achieved. The resulted fixed SRG patterns showed high stability at high temperatures and insolubility in solvents.

Chapter 3 involved a new concept called photoinduced dewetting. Dendritic materials namely D6, D8, D10 and D12 were used for this particular purpose. For shorter spacer azobenzene dendrimers as D6 and D8, we observed dewetting behavior, but not for longer ones as D10 and D12. We proposed this photoinduced dewetting mechanism to increase the mobility of azobenzene derivatives during the formation of SRG.

In the Chapter 4, as a hybrid photoinduced SRG and photoinduced dewetting, a new hierarchical SRG formation method was introduced. We got 3 typical SRG

patterns differ from the classic ones. There are multi column brush liked, single column crocodile liked and another double column shapes. We proved that the cause of their morphological difference can be an attribution of their initial film thickness.

Publication List

1. Wenhan Li, Shusaku Nagano and Takahiro Seki, Photo-crosslinkable liquid-crystalline azo-polymer for surface relief gratings and persistent fixation. *New J. Chem.*, 33, 1343-1348. (2009).
2. Wenhan Li, Shusaku Nagano, Koichiro Yonetake, and Takahiro Seki, Photoinduced dewetting in thin films of liquid crystalline dendritic azobenzene derivatives. *Mol. Cryst. & Liq. Cryst.*, in press. (2011)
3. Wenhan Li, Shusaku Nagano, Koichiro Yonetake, and Takahiro Seki, Hierarchical Structure Formation in SRG Process of Azobenzene Dendrimers. In preparation.

Acknowledgments

This work was carried out at Seki lab in the Department of Molecular Design and Engineering, Graduate School of Engineering, Nagoya University, during 2007-2012.

I am sincerely and heartily grateful to my supervisor, Professor Takahiro Seki, whose encouragement, guidance and support from the initial to the final level enabled me to develop an understanding of the subject. Also I owe my deepest gratitude to Professor Yukikazu Takeoka and Professor Shusaku Nagano, I am sure it would not have been possible without their help. And I am truly indebted and thankful to my colleague Shun Mitsui for his technical assistance.

Besides, I would like to show my gratitude to all the colleagues in Seki laboratory for their friendship and all the colleagues in Yonetake laboratory of Yamagata University for the kindly cooperation.

Meanwhile, it is a great honor for me to give my thanks to the G-COE program for various supports.

Lastly, I offer my best regards and blessings to Professor Eiji Yashima and Professor Zetsu Nobuyuki for my dissertation committee.

January, 2012

Wenhan LI